

Sedentary behavior in mice induces metabolic inflexibility by suppressing skeletal muscle pyruvate metabolism

Piyarat Siripoksup, ... , Jared Rutter, Katsuhiko Funai

J Clin Invest. 2024. <https://doi.org/10.1172/JCI167371>.

Research In-Press Preview Metabolism

Carbohydrates and lipids provide the majority of substrates to fuel mitochondrial oxidative phosphorylation (OXPHOS). Metabolic inflexibility, defined as an impaired ability to switch between these fuels, is implicated in a number of metabolic diseases. Here we explore the mechanism by which physical inactivity promotes metabolic inflexibility in skeletal muscle. We developed a mouse model of sedentariness, small mouse cage (SMC) that, unlike other classic models of disuse in mice, faithfully recapitulated metabolic responses that occur in humans. Bioenergetic phenotyping of skeletal muscle mitochondria displayed metabolic inflexibility induced by physical inactivity, demonstrated by a reduction in pyruvate-stimulated respiration (JO_2) in absence of a change in palmitate-stimulated JO_2 . Pyruvate resistance in these mitochondria was likely driven by a decrease in phosphatidylethanolamine (PE) abundance in the mitochondrial membrane. Reduction in mitochondrial PE by heterozygous deletion of phosphatidylserine decarboxylase (PSD) was sufficient to induce metabolic inflexibility measured at the whole-body level, as well as at the level of skeletal muscle mitochondria. Low mitochondrial PE in C2C12 myotubes was sufficient to increase glucose flux towards lactate. We further implicate that resistance to pyruvate metabolism is due to attenuated mitochondrial entry via mitochondrial pyruvate carrier (MPC). These findings suggest a mechanism by which mitochondrial PE directly regulates MPC activity to modulate metabolic flexibility in mice.

Find the latest version:

<https://jci.me/167371/pdf>



1 **Sedentary behavior in mice induces metabolic inflexibility by suppressing skeletal**
2 **muscle pyruvate metabolism**

3

4 Piyarat Siripoksup,^{1,2} Guoshen Cao,^{1,3} Ahmad A. Cluntun,^{1,3} J. Alan Maschek,^{4,5} Quentinn
5 Pearce,⁴ Marisa J. Lang,^{1,5} Mi-Young Jeong,^{1,3} Hiroaki Eshima,^{1,7} Patrick J. Ferrara,^{1,5} Precious
6 C. Oporum,^{1,5} Ziad S. Mahmassani,^{1,2,7} Alek D. Peterlin,^{1,5} Shinya Watanabe,^{1,5} Maureen A.
7 Walsh,^{1,2} Eric B. Taylor,⁶ James E. Cox,^{1,3,4} Micah J. Drummond,^{1,2,7} Jared Rutter,^{1,3,8} Katsuhiko
8 Funai.^{1,2,5,7,*}

9

10 ¹Diabetes & Metabolism Research Center, University of Utah, Salt Lake City, Utah, USA.

11 ²Department of Physical Therapy & Athletic Training, University of Utah, Salt Lake City, Utah,
12 USA.

13 ³Department of Biochemistry University of Utah, Salt Lake City, Utah, USA.

14 ⁴Metabolomics Core Research Facility, University of Utah, Salt Lake City, Utah, USA.

15 ⁵Department of Nutrition & Integrative Physiology, University of Utah, Salt Lake City, Utah, USA.

16 ⁶Fraternal Order of Eagles Diabetes Research Center, University of Iowa, Iowa City, Iowa, USA.

17 ⁷Molecular Medicine Program, University of Utah, Salt Lake City, Utah, USA.

18 ⁸Howard Hughes Medical Institute, University of Utah, Salt Lake City, Utah, USA.

19

20 *Correspondence:

21 Katsuhiko Funai, Ph.D.

22 Diabetes & Metabolism Research Center

23 University of Utah

24 15 N, 2030 E, Salt Lake City, UT 84112

25 Phone: (801) 585-1781

26 Fax: (801) 585-0701

27 Email: kfunai@health.utah.edu

28

29 **Conflict of Interest**

30 The authors have declared that no conflict of interest exists.

31

32 **Abstract**

33 Carbohydrates and lipids provide the majority of substrates to fuel mitochondrial oxidative
34 phosphorylation (OXPHOS). Metabolic inflexibility, defined as an impaired ability to switch
35 between these fuels, is implicated in a number of metabolic diseases. Here we explore the
36 mechanism by which physical inactivity promotes metabolic inflexibility in skeletal muscle. We
37 developed a mouse model of sedentariness, small mouse cage (SMC) that, unlike other classic
38 models of disuse in mice, faithfully recapitulated metabolic responses that occur in humans.
39 Bioenergetic phenotyping of skeletal muscle mitochondria displayed metabolic inflexibility
40 induced by physical inactivity, demonstrated by a reduction in pyruvate-stimulated respiration
41 (J_{O_2}) in absence of a change in palmitate-stimulated J_{O_2} . Pyruvate resistance in these
42 mitochondria was likely driven by a decrease in phosphatidylethanolamine (PE) abundance in
43 the mitochondrial membrane. Reduction in mitochondrial PE by heterozygous deletion of
44 phosphatidylserine decarboxylase (PSD) was sufficient to induce metabolic inflexibility
45 measured at the whole-body level, as well as at the level of skeletal muscle mitochondria. Low
46 mitochondrial PE in C2C12 myotubes was sufficient to increase glucose flux towards lactate.
47 We further implicate that resistance to pyruvate metabolism is due to attenuated mitochondrial
48 entry via mitochondrial pyruvate carrier (MPC). These findings suggest a mechanism by which
49 mitochondrial PE directly regulates MPC activity to modulate metabolic flexibility in mice.

50

51 **Introduction**

52 Chronic physical inactivity increases all-cause mortality by 30%, accounting for one death every
53 44 seconds (1-4). Sedentary behavior exacerbates the risk for many chronic diseases such as
54 type 2 diabetes and cardiovascular diseases (5-7). Systemic metabolic disturbances induced by
55 inactivity is likely largely responsible for the pathogenesis of these conditions (7, 8). Described
56 often as “metabolic inflexibility”, long-term sedentariness impairs the ability to switch between
57 glucose and fatty-acids to fuel ATP synthesis (9, 10). Metabolic inflexibility that occurs with
58 physical inactivity is primarily driven by the suppression of glucose metabolism in skeletal
59 muscle. Disuse likely directly drives the metabolic reprogramming to attenuate glycolytic flux to
60 mitochondria in the absence of elevated energy demand. The mechanism by which skeletal
61 muscle mitochondrial metabolism adapts to chronic disuse is not well understood.

62
63 Our understanding of the underlying molecular processes that drive inactivity-induced metabolic
64 inflexibility has been limited partly due to the lack of appropriate pre-clinical models of human
65 sedentary behavior (11). Traditional murine models of muscle disuse or physical inactivity, such
66 as hindlimb unloading, cast immobilization, and denervation models are well-suited to study
67 muscle atrophy, but they do not phenocopy the systemic and skeletal muscle metabolic
68 adaptations observed in humans (11, 12). To address this important methodological gap, we
69 adapted a novel mouse model of inactivity, small mouse cage (SMC) (13, 14) that more reliably
70 induces metabolic perturbations with sedentariness in skeletal muscle. This model has now
71 enabled us to more rigorously investigate the interplay between mitochondrial energetics and
72 metabolic inflexibility in the context of physical inactivity.

73
74 Previously, we identified mitochondrial phosphatidylethanolamine (PE) to be an important
75 regulator of mitochondrial oxidative phosphorylation (OXPHOS) in skeletal muscle that is
76 induced by exercise training and suppressed with hindlimb unloading (15). PE is highly

77 concentrated in the inner mitochondrial membrane (IMM) and is autonomously synthesized by
78 phosphatidylserine decarboxylase (PSD) (16, 17). In mammalian systems, nearly all PE is
79 synthesized in the IMM by PSD and exported to other regions of the cell, while the PE
80 generated by the CDP-ethanolamine pathway in the endoplasmic reticulum does not translocate
81 to mitochondria (18, 19). Human mutation in the *PISD* gene, which encodes for the PISD
82 enzyme, causes mitochondrial disease (20-22). We have previously shown that skeletal muscle-
83 specific deletion of PSD (homozygous knockout) in mice is lethal due to robust atrophy and
84 weakness of the diaphragm muscle (15). The consequence of a more modest reduction of
85 mitochondrial PE, such that occurs with sedentariness, is unknown. Importantly, muscle
86 phospholipid composition, particularly low PE, has been linked to metabolic inflexibility in
87 humans (23-26).

88

89 In this study, we implicate reduced muscle mitochondrial PE as the driving force behind
90 inactivity-induced metabolic inflexibility. SMC intervention modestly lowered mitochondrial PE,
91 concomitant to reduced glucose metabolism. We then recapitulated moderate reductions in
92 mitochondrial PE using a skeletal muscle-specific heterozygous knockout of PSD (PSD-Mhet).
93 Unlike their homozygous counterparts, heterozygous deletion of PSD produced modest
94 systemic and skeletal muscle phenotype that resembled many metabolic shifts found with the
95 SMC intervention.

96

97 **Results**

98 **SMC housing induces metabolic inflexibility in male but not female mice**

99 Sedentary behavior promotes systemic and skeletal muscle metabolic inflexibility in humans (7,
100 27). In contrast, commonly utilized models of disuse in mice such as hindlimb unloading
101 increases skeletal muscle glucose uptake (Figure S1A). To better model the metabolic
102 disturbances observed in human inactivity, we developed a mouse model of physical inactivity

103 using SMC (Figure 1A). Male and female wild-type C57BL/6J mice were ambulatory or
104 subjected to eight weeks of SMC housing that substantially restricted gross spontaneous
105 movement (Figure 1B). Body mass, lean mass, and individual muscle masses were significantly
106 reduced in male mice and not in female mice (Figure 1C&D, Figure S1B). In contrast, SMC
107 intervention did not alter adiposity in either sex, although there was a trend for greater adipose
108 tissue masses only in female mice (Figure S1C&D). To evaluate the effects of reduced activity
109 on metabolic flexibility, mice underwent indirect calorimetry for measurements of whole-body O₂
110 consumption (VO₂) and respiratory exchange ratio. VO₂ was not influenced with SMC in both
111 sexes (Figure 1E&F), consistent with findings that changes in physical activity do not drive
112 changes in total daily energy expenditure (28). RER is an indicator of systemic substrate
113 preference, where a value of 1.0 signifies a 100% reliance on carbohydrates, whereas a value
114 of 0.7 indicates a 100% reliance on lipids. Mice rely more on lipids during the light cycle when
115 they are asleep and shift to carbohydrate utilization during the dark cycle when they are active
116 or eating. Notably, while SMC induced metabolic inflexibility in male mice, female mice
117 demonstrated normal metabolic flexibility (Figure 1G&H, Figure S1E&F). Specifically, SMC
118 reduced the ability of male mice to shift to carbohydrate usage during the dark cycle. Further,
119 consistent with attenuated systemic glucose metabolism, SMC intervention elevated fasting
120 serum glucose in male mice (Figure 1I) without alterations in serum insulin levels (Figure S1G).

121
122 To examine glucose metabolism in skeletal muscle, we excised soleus muscles from male and
123 female sham or SMC mice for the measurement of ex vivo 2-deoxyglucose uptake. Congruent
124 with systemic metabolic inflexibility, SMC intervention reduced glucose uptake in both basal and
125 insulin-stimulated conditions in males, but not in females (Figure 1J). These changes in muscle
126 glucose uptake occurred in the absence of changes in total GLUT4 content (Figure 1K). These
127 findings are consistent with the hypothesis that reduced skeletal muscle glucose metabolism
128 drives systemic metabolic inflexibility induced by SMC. It is noteworthy that male mice became

129 metabolically inflexible despite no increases in adiposity (Figure S1C&D). Metabolic inflexibility
130 also occurred independently of increases in food intake or serum cortisol levels. (Figure 1L and
131 Figure S1H). Glucose tolerance was not different between sham and SMC groups in male or
132 female mice (Figure S1I-L). These results are consistent with findings from human bed rest
133 studies (29), where no differences in systemic glucose tolerance was found with bed rest in lean
134 healthy young males. We interpret these findings to mean that reduced skeletal muscle glucose
135 uptake precedes robust changes in systemic glucose metabolism, which can be detected with
136 RER but not with glucose tolerance test at this particular timepoint.

137
138 We sought to capitalize on the sexually dimorphic response to explore the mechanism by which
139 SMC induces skeletal muscle metabolic inflexibility only in male mice. RNA sequencing of
140 gastrocnemius muscles followed by KEGG pathway analysis revealed similarities and
141 differences in gene set enrichment in a number of pathways between males and females
142 (Figure 2A). The ribosomal pathway was among the most negatively enriched categories with
143 both sexes, consistent with the notion that inactivity decreases muscle protein synthesis (30).
144 Notably, metabolic pathways were reduced in males but not in females, suggesting that
145 metabolic reprogramming induced by SMC may be unique to males. Given the central role of
146 mitochondria in these pathways, we further examined the effects of SMC on skeletal muscle
147 mitochondria.

148
149 **SMC housing reduces pyruvate-dependent respiration without altering palmitate-**
150 **stimulated respiration**

151 Previous reports suggest that reduced muscle mitochondrial content can potentially drive
152 metabolic inflexibility induced by inactivity (7, 29). However, our SMC intervention did not alter
153 mitochondrial density in skeletal muscle regardless of sex (Figure 2B&C, Figure S2A), indicating
154 that lower mitochondrial content is not necessary for inactivity-induced suppression of skeletal

155 muscle glucose metabolism (31). Combined with data from RNAseq that expressions of genes
156 in mitochondrial pathways are reduced with SMC suggest that the influence of physical inactivity
157 on mitochondria can be more nuanced. To this end, we further examined respiratory function
158 per unit of mitochondria isolated from gastrocnemius muscle, which represents a muscle with
159 mixed fiber-type composition. High-resolution respirometry experiments showed that SMC
160 diminished respiration (JO_2) driven by pyruvate in male, but not female mice (Figure 2D),
161 consistent with the notion that metabolic inflexibility is driven by mitochondria's ability to accept
162 glycolytic substrates. Strikingly, there was no difference in JO_2 fueled by palmitate (Figure 2E),
163 indicating that the reduced ability of mitochondria to accept substrates is limited to glycolytic
164 substrates. Moreover, these changes occurred independently of changes in OXPHOS protein
165 abundance per unit of mitochondria (Figure 2F, Figure S2B).

166
167 Some studies indicate that mitochondrial electron leak can promote oxidative stress to suppress
168 glucose metabolism (32). Multiple labs including our group have reported that traditional models
169 of disuse promote oxidative stress in skeletal muscle (33, 34). However, our SMC intervention
170 did not alter the ratio of reduced to oxidized glutathione (GSH:GSSG) (Figure 2G) nor reactive
171 lipid aldehydes such as 4-hydroxynonenal (4-HNE) (Figure S2C&D), demonstrating that
172 physical inactivity induced by SMC does not promote oxidative stress. Using high-resolution
173 fluorometry, we further confirmed mitochondrial electron leak (JH_2O_2/JO_2) to be unaltered with
174 the SMC intervention (Figure 2H). These findings are consistent with results from human bed
175 rest studies (35, 36), ruling out oxidative stress as a mechanism by which SMC intervention
176 suppresses skeletal muscle glucose metabolism.

177
178 What is the mechanism by which physical inactivity selectively suppresses mitochondrial
179 pyruvate metabolism in skeletal muscle? SMC intervention had no effect on mRNA levels of
180 pyruvate/glucose metabolism and TCA cycle, nor on protein levels of enzymes of pyruvate

181 metabolism (Figure 3A-C, Figure S2E), indicating that reductions in pyruvate oxidation cannot
182 be attributed to changes in these enzymes. SMC also did not decrease enzyme activities for
183 skeletal muscle pyruvate dehydrogenase, phosphofructokinase, or citrate synthase in male mice
184 (Figure S2F-H). Mitochondrial membrane lipids are known to alter the activity of mitochondrial
185 enzymes in multiple tissues including skeletal muscle (15, 36). Particularly, disuse induced by
186 hindlimb unloading reduces mitochondrial PE in skeletal muscle (15). Thus, we examined the
187 effect of SMC housing on the skeletal muscle mitochondrial lipidome. Using LC-MS/MS, we
188 quantified a total of 243 lipids from isolated mitochondria of gastrocnemius muscles of sham
189 and SMC mice. Analyses of these lipids revealed a trend for an overall reduction ($P = 0.118$) in
190 total phospholipid abundance with SMC in males but not in females (Figure S3A) ($P = 0.789$).
191 73 out of the 243 lipids were significantly downregulated with SMC in male mice (zero
192 upregulated lipids) (Figure S3B) while only two reached statistical significance in female mice
193 (Figure S3C). Among these lipids, mitochondrial PE was most robustly disproportionately
194 downregulated in male SMC mice (Figure 3D&E, Figure S3D), consistent with our previous
195 findings with that of hindlimb unloading (15). Reduced PE with SMC was specific to
196 mitochondria and not reflected in total cellular PE content (Figure S3E&F). The observation that
197 SMC reduced mitochondrial PE in only male mice is likely contributed by males trending to
198 having greater mitochondrial PE to start out with (Figure S3G). In turn, this may contribute to the
199 lack of SMC-induced phenotype in female mice. Mitochondrial PE is almost exclusively
200 generated by the enzyme PSD from PS. SMC did not influence the abundances of
201 mitochondrial PS (nor an alternate PE precursor lyso-PE) (Figure S3H-K). Nevertheless, SMC
202 substantially reduced the abundance of PSD mRNA in skeletal muscle (Figure 3F). Thus, we
203 proceeded to investigate the role that mitochondrial PE may play in metabolic inflexibility
204 induced by physical inactivity.

205

206 **Muscle PSD haploinsufficiency makes mice more susceptible to inactivity-induced**
207 **metabolic inflexibility**

208 Previously, we demonstrated that homozygous deletion of muscle PSD causes lethality due to
209 metabolic and contractile failure in the diaphragm muscle (15). Homozygous deletion promotes
210 a reduction in mitochondrial PE that is far more robust in magnitude compared to changes in
211 mitochondrial PE observed with SMC. To model a more modest reduction in skeletal muscle
212 mitochondrial PE, we studied mice with tamoxifen-inducible muscle-specific PSD heterozygous
213 deletion (PSD-Mhet; PSD^{f/f} and HSA-MerCreMer^{+/-}) (Figure 4A). As designed, skeletal muscle
214 from PSD-Mhet mice had reduced PSD mRNA abundance compared to controls (PSD-Mhet;
215 PSD^{f/f} and HSA-MerCreMer^{-/-}) (Figure 4B), as well as modest depletions in some species of
216 mitochondrial PE (Figure 4C, Figure S4A) in male mice. Heterozygous deletion of PSD was not
217 sufficient to significantly reduce mitochondrial PE in female mice. Unlike the PSD homozygous
218 knockout mice, PSD-Mhet appeared normal and healthy under unstressed conditions (Figure
219 S4B-I). However, PE haploinsufficiency was sufficient to impair mitochondrial energetics under
220 pyruvate-stimulated conditions (Figure S4J), but not palmitate-induced conditions (Figure S4K)
221 under sham conditions but was not adequate to attenuate skeletal muscle 2-deoxyglucose
222 uptake in soleus muscles (Figure S4L). Taken together, these results suggest sufficiency for PE
223 to alter maximal skeletal muscle respiration, but not necessary to cause metabolic inflexibility
224 under sham conditions.

225
226 We placed control and PSD-Mhet male mice on eight weeks of SMC to study their systemic and
227 skeletal muscle metabolism. Muscle PSD haploinsufficiency did not influence body mass, body
228 composition, food intake, serum cortisol, or masses of skeletal muscle and adipose tissues
229 (Figure 4D-F, Figure S4M-O). Indirect calorimetry of these mice showed a slight reduction in
230 whole-body VO₂ in PSD-Mhet compared to controls (Figure 4G), which was not explained by
231 changes in physical activity (both virtually undetectably low with SMC). Consistent with our

232 hypothesis that low mitochondrial PE may drive metabolic inflexibility, RER data revealed
233 suppression of glucose metabolism during dark cycle in PSD-Mhet mice compared to control
234 mice (Figure 4H; Figure S4P). Neither fasting glucose nor glucose tolerance was different
235 between the groups (Figure 4I&J). However, circulating insulin levels at the 30-minute timepoint
236 of the glucose tolerance test was higher in PSD-Mhet compared to controls (Figure 4K),
237 suggesting that PSD haploinsufficiency may require greater circulating insulin to stimulate
238 muscle glucose metabolism. Indeed, skeletal muscle glucose uptake was attenuated in PSD-
239 Mhet mice compared to control mice (Figure 4L). Collectively, these results suggest that muscle
240 PE deficiency may impair skeletal muscle glucose metabolism to promote metabolic inflexibility.

241
242 Similar to our results with the SMC intervention in wildtype mice, PSD haploinsufficiency did not
243 alter mitochondrial content in skeletal muscle (Figure 5A&B, Figure S5A). High-resolution
244 respirometry experiments revealed that low mitochondrial PE coincides with reduced pyruvate-
245 stimulated JO_2 , without affecting OXPHOS protein content per unit of mitochondria (Figure 5C-
246 E, Figure S5B). Unlike homozygous deletion of PSD (15), heterozygous knockout of PSD did
247 not promote oxidative stress or mitochondrial electron leak (Figure 5F-H, Figure S5C). Taken
248 together, these findings are consistent with the notion that low mitochondrial PE is sufficient to
249 drive systemic and skeletal muscle metabolic inflexibility. In addition to physical inactivity, high-
250 fat diet feeding is also known to induce metabolic flexibility (37). However, phenotypes for
251 whole-body glucose metabolism or skeletal muscle mitochondrial function were not different
252 between control and PSD-Mhet mice after high-fat diet feeding (Figure S6A-P). These
253 observations suggest that reduction in mitochondrial PE influences metabolic flexibility by acting
254 on pathways that are activated during physical inactivity but not with high-fat diet feeding. To
255 delve deeper into the mechanism by which mitochondrial PE abundance facilitates pyruvate
256 metabolism, we performed additional experiments in murine C2C12 myotubes.

257

258 **Mitochondrial PE deficiency impairs pyruvate metabolism**

259 To study the effects of low mitochondrial PE, C2C12 myotubes were subjected to lentivirus-
260 mediated knockdown with shRNA encoding either scrambled (shSC) or PSD (shPSD), which
261 was confirmed by quantitative real-time polymerase chain reaction (RT-qPCR) (Figure 6A). We
262 took advantage of the slow turnover rate for phospholipid molecules and performed all
263 experiments 3 days post-lentiviral infection to model modest reductions in some mitochondrial
264 PE species (Figure 6B; Figure S7A). Consistent with our observations *in vivo*, PSD knockdown
265 attenuated pyruvate-stimulated JO_2 or JATP (Figure 6C&D), but not palmitate-stimulated JO_2
266 (Figure 6E). PSD knockdown also had no effect on OXPHOS content (total cellular or
267 mitochondrial), mitochondrial electron leak, or oxidative stress (Figure 6F, Figure S7B-G).
268 These findings indicate that cell-autonomous effects of PSD deletion are responsible for the
269 phenotype observed *in vivo*.

270
271 Knockdown of PSD very strikingly accelerated the yellowing of the culture medium compared to
272 shSC cells (Figure 6G). Yellowing of cell culture media is usually indicative of higher
273 acidification rate due to lactate production (38). Indeed, lactate concentration in the media was
274 substantially elevated in shPSD cells compared to shSC controls (Figure 6H), and analysis of
275 C2C12 myotubes on the Seahorse Bioanalyzer revealed increased extracellular acidification
276 (ECAR) rate with PSD deletion (Figure 6I). Together, these data likely indicate that low PE
277 causes mitochondria to become resistant to pyruvate metabolism (39, 40).

278
279 To more closely examine intracellular pyruvate metabolism, we performed stable isotope tracing
280 using uniformly labeled ^{13}C -glucose (Figure 7A-H, Figure S8). Targeted mass spectrometry
281 analyses revealed that labeling for glycolytic metabolites leading up to pyruvate was elevated
282 with PSD knockdown (Figure 7B&C), suggesting that low mitochondrial PE does not
283 compromise glucose-to-pyruvate metabolism. Consistent with increased lactate concentration in

284 the media, lactate labeling was higher in shPSD cells compared to shSC (Figure 7D). In
285 contrast, low mitochondrial PE was not associated with increased labeling towards TCA
286 intermediates (Figure 7E-H), suggesting that flux towards lactate, and not TCA cycle, explains
287 the increased labeling for the glycolytic metabolites. Similarly, circulating lactate was greater in
288 SMC PSD-Mhet mice compared to SMC control mice (Figure 8A). These findings are consistent
289 with the notion that mitochondrial PE deficiency impairs mitochondrial pyruvate metabolism.

290

291 **Mitochondrial PE facilitates mitochondrial pyruvate entry**

292 We sought to identify the mechanism by which low mitochondrial PE attenuates pyruvate
293 metabolism. Surprisingly, PSD deletion did not reduce protein or mRNA abundance of
294 mitochondrial pyruvate carriers (MPC1 and MPC2) or pyruvate dehydrogenase (PDH) (Figure
295 8B, Figure S9A-C), suggesting that attenuated pyruvate metabolism is not explained by
296 changes in abundance of these proteins. In fact, there was a statistically significant increase in
297 LDH and a trend for an increase in PDH with PSD deletion. PSD is localized at the inner
298 mitochondrial membrane to generate PE. Thus, we reasoned that the mitochondrial PE may
299 regulate the activity of MPC, which also resides in the inner mitochondrial membrane (41, 42).

300

301 To test this possibility, we took a two-pronged approach to link MPC to a defect in pyruvate
302 metabolism (Figure 8C). First, we performed pyruvate-stimulated respirometry with or without
303 the MPC inhibitor UK-5099 (43). Consistent with UK-5099's action on MPC, pyruvate-stimulated
304 JO_2 was significantly reduced in shSC myotubes (Figure 8D). As expected, MPC inhibition did
305 not completely suppress JO_2 due to anaplerosis. Strikingly, MPC-inhibited JO_2 in shSC cells
306 were similar to JO_2 in shPSD cells without UK-5099, consistent with the notion that reduced JO_2
307 in shPSD cells is due to attenuated MPC activity. Furthermore, UK-5099 had no effect on JO_2 in
308 shPSD cells, confirming that residual JO_2 in shPSD cells is independent of pyruvate entry via
309 MPC. Second, we compared JO_2 in response to pyruvate or methyl-pyruvate (MePyr). MePyr is

310 a pyruvate-analog that can bypass the MPC, diffuse freely into the mitochondrial matrix, and
311 subsequently demethylated to become mitochondrial pyruvate (44). MePyr rescued JO_2 in
312 shPSD myotubes to pyruvate-stimulated JO_2 levels in shSC cells (Figure 8E). Taken together,
313 these findings suggest that low mitochondrial PE attenuates MPC activity to inhibit mitochondrial
314 pyruvate metabolism.

315

316 **Discussion**

317 Skeletal muscle disuse or physical inactivity is linked to 35 chronic diseases (4, 45). Many of
318 these conditions are attributed to metabolic disturbances caused by sedentary behavior.

319 Nevertheless, the mechanisms by which physical inactivity alters systemic and skeletal muscle
320 metabolism have been poorly defined, likely due to the lack of pre-clinical models (11, 12). In
321 this study, we developed a novel mouse model of inactivity that reliably induces metabolic
322 inflexibility in male C57BL/6J mice. Metabolic inflexibility was likely driven by pyruvate
323 resistance in skeletal muscle mitochondria. We implicate inactivity-induced downregulation of
324 mitochondrial PE as a driver of pyruvate resistance. Mice with skeletal muscle-specific deletion
325 of PSD upon SMC insult was sufficient to recapitulate metabolic inflexibility and mitochondrial
326 pyruvate resistance *in vivo* and *in vitro*. Using stable isotope tracing and high-resolution
327 respirometry, we demonstrate that PE likely directly acts on MPC to facilitate mitochondrial
328 pyruvate entry.

329

330 Oxidative stress has been implicated in pathogenesis of inactivity-induced metabolic inflexibility
331 (4, 45). Indeed, skeletal muscle oxidative stress is commonly manifested in many of the
332 traditional models of mouse disuse (11, 12). However, while these models are useful in studying
333 muscle atrophy, mice do not develop systemic and skeletal muscle metabolic adaptation
334 observed with human sedentary behavior (11, 12). In our newly developed SMC model,
335 metabolic inflexibility and suppression of glucose metabolism were similar to that of human bed

336 rest studies, but muscles from this model of inactivity did not exhibit oxidative stress
337 (glutathione, lipid hydroperoxides, mitochondrial electron leak). Notably, our findings from the
338 SMC model reconcile with results from human bedrest studies that oxidative stress cannot
339 explain metabolic inflexibility (36).

340

341 Previously we demonstrated that muscle mitochondrial PE becomes elevated with exercise
342 training and decreased with hindlimb unloading (15). There are no studies that examined
343 muscle mitochondrial PE in humans, but total cellular PE has been linked with insulin sensitivity
344 [27]. In subjects with type 2 diabetes, muscle PE content was lower compared to obese normo-
345 sensitive individuals. We have previously demonstrated the role of PE generated by the
346 Kennedy pathway (46, 47), where suppression of PE synthesis at ER increased, not decreased,
347 skeletal muscle insulin sensitivity with high-fat feeding. There is evidence that syntheses of PE
348 at ER or mitochondria might become upregulated to compensate each other (46), which might
349 contribute to phenotypes found in these papers. Together, these findings highlight the complex
350 interactions between muscle glucose metabolism and subcellular lipid metabolism. They also
351 reinforce the notion that PE generated at ER and mitochondria do not mix with each other.

352

353 Unlike oxidative stress, SMC reduced skeletal muscle mitochondrial PE concomitant to the
354 development of metabolic inflexibility. What are the mechanisms by which exercise or inactivity
355 promotes changes in muscle mitochondrial PE? In our previous study, as well as in the current
356 study, changes in mitochondrial PE coincided with mRNA abundance of PSD, an enzyme that
357 generates PE in the inner mitochondrial membrane. We believe that changes in PSD levels
358 likely drive the changes in mitochondrial PE abundance. It is currently unknown whether PSD
359 activity is regulated by post-translational modification. It is also possible that there are changes
360 in the upstream mechanism for mitochondrial PE synthesis. PSD generates PE from
361 mitochondrial PS, which is synthesized by PS synthase 1 and 2 in the endoplasmic reticulum

362 (48, 49) and transported to mitochondria via Preli3b (50). Finally, it would be important to
363 determine mechanism for the transcriptional control of PSD.
364
365 By an unknown reason, PE generated at the endoplasmic reticulum by the Kennedy Pathway
366 do not enter mitochondria (16). This is exemplified by findings that inhibition of PE synthesis at
367 the ER does not reduce mitochondrial function in skeletal muscle (46, 47). In fact, deletion of
368 ECT (CTP:phosphoethanolamine cytidyltransferase, an intermediate step in PE synthesis)
369 increases mitochondrial content, an observation that may be explained by a compensatory
370 increase in muscle PSD (46). Similarly, deletion of CEPT1 (choline/ethanolamine
371 phosphotransferase, the final step in PE synthesis) increases skeletal muscle glucose
372 metabolism (47). There are two caveats to our data on mitochondrial PE that are worth noting.
373 First, our lipidomic analyses were performed on mitochondrial prep that is not exclusively IMM
374 where MPC resides. They also contain OMM and other organelle contaminants that are also
375 highly abundant in PE. While PSD almost exclusively contributes for PE in IMM, PE in these
376 contaminants are produced by the Kennedy Pathway. Thus, it is very likely that our data on
377 mitochondrial PE underestimates the true concentration of PE in IMM by a meaningful margin. A
378 technological breakthrough to provide spatial resolution on IMM lipids is needed to better
379 understand the exact nature of these changes. Second, it is worth noting that PE species
380 distribution between muscles and C2C12 myotubes are quite different from each other. Acyl-
381 chain combinations on PE is predicted to influence how these lipids influence IMM enzymes as
382 well as membrane properties. The predominant PE species in in vivo appear to contain 22:6 in
383 the sn-2 position, a preferred substrate of PSD, whereas these species are much lower
384 compared to other PE species in C2C12 myotubes. The differences are likely enabled by
385 differences in fatty acid and/or ethanolamine availability between in vitro and in vivo (ZZ
386 Oemer). Overall, combined with our previous report on muscle-specific homozygous deletion of
387 PSD (15), the current study emphasizes that the mitochondrial PE pool remains distinct from

388 that of the endoplasmic reticulum. This is also consistent with findings in yeast, as PE generated
389 by PSD with a forced localization at the outer mitochondrial membrane or endoplasmic
390 reticulum have differential cellular consequences (51).

391

392 On a similar note, one of the critical findings of this study was that low mitochondrial PE
393 coincided with pyruvate resistance, but not with palmitate-stimulated JO_2 . We demonstrate that
394 PE likely directly facilitates MPC to promote mitochondrial pyruvate uptake, which takes place
395 across the inner mitochondrial membrane where PE is enriched. Meanwhile, the rate-limiting
396 step for fatty acid oxidation is at the step of carnitine palmitoyl transferase-1 (CPT1), which is
397 localized on the outside of the outer mitochondrial membrane (52). Not only is CPT1 not a
398 transmembrane protein, but it is also localized at the outer mitochondrial membrane where PE
399 is less concentrated (53). The enzyme equivalent to the MPC for fatty acid oxidation is
400 carnitine/acylcarnitine translocase which is located in the inner mitochondrial membrane, but
401 this enzyme is not the rate-limiting step of palmitate entry nor palmitate oxidation (54, 55). Thus,
402 we believe that differential subcellular localization of the rate-limiting step for pyruvate or
403 palmitate oxidation contributes to the disproportionate influence of low mitochondrial PE on
404 substrate preference.

405

406 Yellowing of cell culture media was the most apparent and robust phenotype observed with
407 PSD knockdown *in vitro*. Our flux experiments reveal that this is a direct result of accelerated
408 flux of glucose towards lactate. Experiments with UK-5099 and MePyr suggest that pyruvate
409 resistance in PSD deficient cells are attributed to the effects of PE on MPC. Multiple studies
410 show that inhibition of MPC promotes resistance for mitochondria to oxidize glycolytic
411 substrates (41, 42, 56, 57). We believe that the effects of PE deficiency on MPC is the
412 mechanism behind the metabolic inflexible phenotype observed in PSD-Mhet mice. We further
413 reason that metabolic inflexibility caused by sedentariness is attributed to low mitochondrial PE

414 which in turn reduces mitochondrial pyruvate entry. It would be important for future studies to
415 elucidate whether PE directly affects the stability of MPC or its post-translational modifications
416 to regulate pyruvate entry.

417

418 Lactate infusion is known to rapidly suppress insulin-stimulated glycolysis and intracellular
419 glucose metabolism that leads to a decrease in glucose uptake (58). Likewise, we speculate
420 that low mitochondrial PE attenuates pyruvate import and oxidation, suppressing intracellular
421 glycolytic flux to reduce glucose uptake. Nonetheless, the effects of physical inactivity on whole-
422 body and skeletal muscle metabolism are pleiotropic and we cannot effectively rule out the
423 contribution of alternate mechanisms that underlie reduced glucose transport with SMC.

424

425 In conclusion, the current study demonstrates a novel mechanism by which PE facilitates
426 mitochondrial pyruvate entry. We show that a modest reduction in mitochondrial PE is sufficient
427 to promote resistance towards pyruvate oxidation both *in vitro* and *in vivo*. These observations
428 were further extrapolated by findings that pyruvate resistance can be rescued by the membrane
429 permeable MePyr, and that the MPC inhibitor UK-5099 can phenocopy the effects of low
430 mitochondrial PE. We propose that this process drives the metabolic inflexibility induced by
431 physical inactivity in male mice. Resistance to pyruvate oxidation may represent a selective
432 advantage for mammals in a state of reduced energy demand, such that substrates are shunted
433 away from skeletal muscle and stored away for subsequent energetic needs. In the modern age
434 of abundant food supply, inactivity-driven resistance for glycolytic substrates can exacerbate the
435 development of metabolic diseases.

436

437 **Limitations**

438 The physiological responses that occur as a result of physical inactivity are highly complex and
439 appear to be sex dependent. The majority of human best rest or reduced activity studies have

440 largely been conducted in males (7, 27, 36, 59), while inactivity studies in females have focused
441 on post-menopausal women (60, 61). In our study, female mice were resistant to SMC-induced
442 metabolic inflexibility. The cause for this difference is unclear, but our findings suggest that
443 muscle mitochondria from male mice contained higher PE compared to female mice in sham
444 condition, such that they were more prone to inactivity-induced reduction in mitochondrial PE
445 and suppression of mitochondrial pyruvate metabolism. It is unclear whether such sexual
446 dimorphic response persists in humans. We believe that more studies examining both sexes, in
447 humans and in mice, are needed to study the influence of sedentary behavior on metabolic
448 homeostasis.

449

450 **Methods**

451 ***Sex as a biological variable***

452 Both male and female mice were examined. Differences between sexes were extrapolated to
453 study mechanisms.

454

455 ***Animals***

456 Eight-week old C57BL/6J mice were purchased from the Jackson Laboratory (Strain# 000664)
457 for initial small mouse cage experiments. Heterozygous PSD-Mhet mice were generated by
458 crossing our conditional PSD knockout (PSDcKO^{+/+}) mice (previously described (15)).
459 PSDcKO^{+/+} mice harbor loxP sites flanking exons 4 to 8 of the mouse PSD gene. These mice
460 were crossed with HSA-MerCreMer mice (HSA-MerCreMer, tamoxifen inducible α -human
461 skeletal actin Cre, courtesy of K. Esser, University of Florida). All mice were bred onto
462 C57BL/6J background and were born at normal Mendelian ratios. Tamoxifen (final
463 concentration of 10 mg ml⁻¹) is injected intraperitoneally (7.5 μ L/g of bodyweight) to PSD-Mhet
464 mice and their respective controls for 5 consecutive days. After 2 weeks washout, mice were
465 studied as sham, SMC (discussed further below), or high-fat diet feeding (Western diet, TD.
466 88137, Envigo) groups. It is noteworthy that because tamoxifen is an estrogen receptor
467 antagonist that may influence metabolism. Thus, data from mice injected with tamoxifen (control
468 and PSD-Mhet mice) to those that have not (wildtype mice with or without MSC) may not always
469 be directly comparable. Differences in housing facility, age, and dates of experiments also
470 contribute to these differences. Mice were maintained on a 12-hour light/12-hour dark cycle in a
471 temperature-controlled room at 22°C. All animals were fasted for 4 hours prior to tissue
472 collection or experiments. Prior to all terminal experiments and tissue harvesting, mice were
473 given an intraperitoneal injection of 80 mg/kg ketamine and 10 mg/kg xylazine. All protocols
474 were approved by Institutional Animal Care and Use Committee at the University of Utah.

475

476 ***Small mouse cage***

477 Modified and further developed from Mahmassani et al. (14) and Marmonti et al. (13), SMC is a
478 rectangular box produced from acrylic plastic, made at the University of Utah's Machine Shop
479 Core. Bedding is placed one-third of the height leaving 4 cm of clearance height. Air holes are
480 designed on all four sides to facilitate air circulation. One air hole on the side was plugged with a
481 Hydropac water lixit (Lab Products Inc., Seaford, Delaware) providing water ad libitum and one
482 air hole on the top is compatible with the hydration system of the Columbus Instruments
483 Oxymax Lab Animal Monitoring System (CLAMS) for determination of whole animal energy
484 expenditure. Abundance of food is provided on top of the bedding to allow ad libitum food
485 consumption. Variable water leakage and crumbling of food are caveats to the attainment of
486 accurate food and water intake in the SMC. Bedding, food, and water were changed every 2-3
487 days to ensure cleanliness. Two SMC cages can fit in one regular mouse cage. Some
488 experiments were performed with sham or SMC mice housed in pairs, while other experiments
489 were performed with separate cages for sham or SMC mice.

490

491 ***Indirect Calorimetry***

492 The Columbus Instruments Lab Monitoring System were used to measure VO_2 , RER
493 (respiratory exchange ratio, VCO_2/VO_2), food intake, and physical activity (for sham animals
494 only) of sham and SMC mice during Week 7 or 8 of SMC. Mice were individually caged and
495 acclimated for over 24 h in the system before data were collected. Body composition was
496 determined using the Bruker Minispec NMR (Bruker).

497

498 ***Glucose tolerance test***

499 Intraperitoneal glucose tolerance tests were performed by injection of 1 mg glucose per gram
500 body mass during Week 8 of SMC, at least 3 days prior to sacrifice. Mice were fasted for 4
501 hours prior glucose injection. Blood glucose was measured before glucose injection and 15, 30,

502 60, and 120 minutes after injection via tail bleed with a handheld glucometer (Bayer Contour
503 7151H). In a separate set of experiments, mice were injected with 1 mg glucose per gram body
504 mass, and blood was taken from the facial vein at the 30-minute time point for insulin
505 quantification.

506

507 ***Ex vivo skeletal muscle [³H]2-deoxy-D-glucose uptake***

508 *Ex vivo* glucose uptake was measured in soleus muscle as previously described (47). In brief,
509 soleus muscles were dissected and placed in a recovery buffer (KHB with 0.1% BSA, 8 mM
510 glucose, and 2 mM mannitol) at 37°C for 10 minutes. After incubation in recovery buffer,
511 muscles were moved to preincubation buffer (KHB with 0.1% BSA, 2mM sodium pyruvate, and
512 6 mM mannitol) with or without 200 µU/mL insulin for 15 minutes for soleus and with or without
513 600 µU/mL insulin for EDL. After preincubation, muscles were placed in incubation buffer (KHB
514 with 0.1% BSA, 9 mM [¹⁴C]mannitol, 1 mM [³H]2-deoxyglucose) with or without 200 µU/mL
515 insulin for 15 minutes. Contralateral muscles were used for basal or insulin-stimulated
516 measurements. After incubation, muscles were blotted dry on ice-cold filter paper, snap-frozen,
517 and stored at –80°C until analyzed with liquid scintillation counting.

518

519 ***Serum insulin, glucose, and cortisol quantification***

520 Blood was collected from facial vein either before anesthesia or at the 30-minute time point of
521 the glucose tolerance test. Blood was then placed at room temperature for 20 minutes to clot
522 prior to centrifugation at 2000 x g for 10 minutes at 4°C. The supernatant (serum) was collected,
523 placed in a new tube, and stored at until –80°C analysis. Serum insulin levels were quantified
524 using a Mouse Insulin ELISA kit (Cat# 90080 Crystal Chem, Chicago, Illinois). Serum glucose
525 was quantified using a Mouse Glucose Assay Kit (Cat# 81692 Crystal Chem, Chicago, Illinois).
526 Serum cortisol levels were quantified by the DetectX ELISA kit (Cat# K003-H1W Arbor assays,
527 Chicago, USA).

528

529 ***High-resolution respirometry and fluorometry***

530 Mitochondrial O₂ utilization was measured using the Oroboros O2K Oxygraphs. Skeletal muscle
531 tissues were minced in mitochondria isolation medium (300 mM sucrose, 10 mM HEPES, 1 mM
532 EGTA) and subsequently homogenized using a Teflon-glass system. Homogenates were then
533 centrifuged at 800 x g for 10 min, after which the supernatant was taken and centrifuged at
534 12,000 x g for 10 min. The resulting pellet was carefully resuspended in mitochondria isolation
535 medium. Isolated mitochondria were then added to the oxygraphy chambers containing assay
536 buffer (MES potassium salt 105 mM, KCl 30 mM, KH₂PO₄ 10 mM, MgCl₂ 5 mM, BSA 0.5
537 mg/ml). Respiration was measured in response to the following substrates: 0.5mM malate, 5mM
538 pyruvate, 5mM glutamate, 10mM succinate, 1.5 μM FCCP, 0.02mM palmitoyl-carnitine, 5mM
539 carnitine. ATP production was measured fluorometrically using a Horiba Fluoromax 4 (Horiba
540 Scientific), by enzymatically coupling ATP production to NADPH synthesis as previously
541 described (62). Respiration and ATP production were measured in the presence of 2mM ADP,
542 unless otherwise stated.

543

544 For inhibitor experiments in mitochondria isolated from shSC and shPSD myotubes, the
545 mitochondrial pyruvate carrier (MPC) inhibitor, UK-5099 (5048170001, Sigma Aldrich), was
546 used to inhibit MPC activity. To induce a submaximal drop of pyruvate-dependent respiration,
547 100 nM UK-5099 was used at a submaximal concentration and injected into the oxygraph
548 chamber following the addition of malate and pyruvate. Respiration was measured in response
549 to the following substrates: 0.5 mM malate, 5 mM pyruvate, 2 mM ADP, and 1 μM FCCP. To
550 evaluate whether pyruvate-dependent respiration was compromised in shSC and shPSD
551 mitochondria, respiration was measured in response to either 5 mM pyruvate or 5 mM methyl
552 pyruvate (371173, Sigma Aldrich) along with the above substrates.

553

554 ***H₂O₂ measurements***

555 Mitochondrial H₂O₂ emission was determined in isolated mitochondria from skeletal muscle. All
556 JH₂O₂ experiments were performed in buffer Z supplemented with 10 mM Amplex UltraRed
557 (Invitrogen), 20 U/mL CuZn SOD, and 25 mM Blebbistatin (for permeabilized muscle fibers
558 only). Briefly, isolated mitochondria or permeabilized fibers were added to 1 ml of assay buffer
559 containing Amplex Ultra Red, which produces a fluorescent product when oxidized by H₂O₂.
560 H₂O₂ emission was measured following the addition of 10mM succinate or 5 mM pyruvate for a
561 final concentration. The appearance of the fluorescent product was measured by a Horiba
562 Fluoromax 4 fluorometer (excitation/emission 565/600).

563

564 ***Seahorse assay***

565 Extracellular acidification rate (ECAR) was measured in C2C12 myoblasts using a Seahorse
566 XF96 Analyzer. Myoblasts were plated at 5 x 10⁴ cells/well and grown in lentiviral media for 48
567 hours. C2C12 cells were selected with puromycin throughout differentiation for 3 days. The real-
568 time extracellular acidification rate (ECAR) was measured using the XFe96 extracellular flux
569 analyzer with the Glycolysis Stress Kit (Agilent Technologies) following the manufacturer's
570 instructions. The measurement was normalized to total protein determined by Pierce BCA
571 Protein Assay Kit (ThermoFisher). Briefly, cells were seeded on XF96 cell culture microplates
572 (Seahorse Bioscience) at a seeding density of 5.0 x 10³ cells per well. Before assay, cells were
573 rinsed twice and kept in pre-warmed XF basic assay medium (pH 7.4) supplemented with 2 mM
574 glutamine in a 37°C non-CO₂ incubator for an hour. Then the rate was measured at 37°C in 14
575 replicates (separate wells) by using the following compounds in succession: 10 mM glucose, 1
576 μM oligomycin, and 50 mM 2-DG. Basal ECAR was measured before drug exposure. The
577 glycolytic function metrics was calculated by Seahorse Wave Desktop Software as directed in
578 the glycolysis stress kit manual (Agilent Technologies).

579

580 **Glutathione**

581 Skeletal muscle GSH and GSSG was measured using the fluorometric GSH/GSSG Ratio
582 Detection Assay Kit II (Abcam 205811). Briefly, whole plantaris muscle was homogenized in
583 lysis buffer containing 0.1% SDS, 0.1% sodium deoxycholate, 1% Triton X-100, 50 mM Tris-HCl
584 pH 7.6, 5 mM EDTA, 150 mM NaCl, and protease and phosphatase inhibitor cocktail,
585 deproteinized using the Deproteinizing Sample Kit – TCA (Abcam 204708), nutated at 4°C for 1
586 hour, and centrifuged at 4°C for 15 min at 12,000g. The supernatant was collected and protein
587 concentrations were determined using the Pierce BCA Protein Assay (Thermo Fischer
588 Scientific). Supernatant was then used to determine GSH and total glutathione. Fluorescence
589 was measured at Ex/Em = 490/520nm with a fluorescence microplate reader.

590

591 **Enzyme activity assays**

592 PDH (Ab109902), PFK (Ab155898), and CS (Ab119692) activity assays were performed
593 utilizing activity assay kits from Abcam.

594

595 **Cell culture**

596 C2C12 myoblasts (ATCC CRL-1772) were grown in high-glucose DMEM (4.5 g/L glucose, with
597 L-glutamine; Gibco 11965-092) supplemented with 10% FBS (heat-inactivated, certified, US
598 origin; Gibco 10082-147), and 0.1% penicillin-streptomycin (10,000 U/mL; Gibco 15140122).

599 C2C12 cells were

600 differentiated into myotubes with low-glucose DMEM (1 g/L glucose with 4mM L-glutamine and
601 110 mg/L sodium pyruvate; Gibco 11885-084) supplemented with 2% horse serum (defined;
602 VWR 16777), and 0.1% penicillin-streptomycin.

603

604 **Lentivirus-mediated knockdown of PSD**

605 PSD expression was decreased using pLKO.1 lentiviral-RNAi system. Plasmids encoding
606 shRNA for mouse PISD (shPSD: TRCN0000115415) was obtained from MilliporeSigma.
607 Packaging vector psPAX2 (ID 12260), envelope vector pMD2.G (ID 12259), and scrambled
608 shRNA plasmid (SC: ID 1864) were obtained from Addgene. HEK293T cells in 10 cm dishes
609 were transfected using 50 μ L 0.1% polyethylenimine, 200 μ L, 0.15 M sodium chloride, and 500
610 μ L Opti-MEM (with HEPES, 2.4 g/L sodium bicarbonate, and l-glutamine; Gibco 31985) with
611 2.66 μ g of psPAX2, 0.75 μ g of pMD2.G, and 3 μ g of either scrambled or PISD shRNA plasmid.
612 Cells were selected with puromycin throughout differentiation to ensure that only cells infected
613 with shRNA vectors were viable.

614

615 ***U-¹³C glucose labeling in cultured myotubes***

616 For metabolite extraction, cold 90% methanol (MeOH) solution was added to each sample to
617 give a final concentration of 80% MeOH to each cell pellet. Samples were then incubated at -20
618 $^{\circ}$ C for 1 hr. After incubation, samples were centrifuged at 20,000 x g for 10 minutes at 4 $^{\circ}$ C. The
619 supernatant was then transferred from each sample tube into a labeled, fresh micro centrifuge
620 tube. Process blanks were made using only extraction solvent and no cell culture. The samples
621 were then dried *en vacuo*.

622

623 All GC-MS analysis was performed with an Agilent 5977b HES fit with an Agilent 7693A
624 automatic liquid sampler. Dried samples were suspended in 40 μ L of a 40 mg/mL O-
625 methoxylamine hydrochloride (MOX) (MP Bio #155405) in dry pyridine (EMD Millipore
626 #PX2012-7) and incubated for one hour at 37 $^{\circ}$ C in a sand bath. 25 μ L of this solution was
627 added to auto sampler vials. 60 μ L of N-methyl-N-trimethylsilyltrifluoroacetamide (MSTFA with
628 1%TMCS, ThermoFisher Scientific #TS48913) was added automatically via the auto sampler
629 and incubated for 30 minutes at 37 $^{\circ}$ C. After incubation, samples were vortexed and 1 μ L of the
630 prepared sample was injected into the gas chromatograph inlet in the split mode with the inlet

631 temperature held at 250 °C. A 10:1 split ratio was used for analysis for the majority of
632 metabolites. Any metabolites that saturated the instrument at the 10:1 split were analyzed at a
633 50:1 split ratio. The gas chromatograph had an initial temperature of 60 °C for one minute
634 followed by a 10 °C/min ramp to 325 °C and a hold time of 10 minutes. A 30-meter Agilent
635 Zorbax DB-5MS with 10 m Duraguard capillary column was employed for chromatographic
636 separation. Helium was used as the carrier gas at a rate of 1 mL/min.

637
638 Data was collected using the Agilent MassHunter software. Metabolites were identified and their
639 peak area was recorded using MassHunter Quant. Metabolite identity was established using a
640 combination of an in-house metabolite library developed using pure purchased standards and
641 the NIST and Fiehn libraries. There are a few reasons a specific metabolite may not be
642 observable through GC-MS. The metabolite may not be amenable to GC-MS due to its size, or
643 a quaternary amine such as carnitine, or simply because it does not ionize well.

644

645 ***Lipid Extraction***

646 LC-MS-grade solvents and mobile phase modifiers were obtained from Honeywell Burdick &
647 Jackson, Morristown, NJ (acetonitrile, isopropanol, formic acid), Fisher Scientific, Waltham, MA
648 (methyl *tert*-butyl ether) and Sigma–Aldrich/Fluka, St. Louis, MO (ammonium formate,
649 ammonium acetate). Lipid standards were obtained from Avanti Polar Lipids, Alabaster, AL.
650 Lipids were extracted from mitochondria using a modified Matyash lipid extraction (63) using a
651 biphasic solvent system of cold methanol, methyl *tert*-butyl ether (MTBE), and water. Briefly, a
652 mixture of cold MTBE, methanol, and internal standards (Mouse SPLASH LIPIDOMIX Avanti
653 Polar Lipids 330707 and Cardiolipin Mix I Avanti Polar Lipids LM6003) were added to isolated
654 skeletal muscle mitochondria isolated mitochondria from C2C12 myotubes or gastrocnemius
655 skeletal muscle. Samples were sonicated for 60 sec, then incubated on ice with occasional
656 vortexing for 1 hr. After addition of 188 µL of PBS, the mixture was incubated on ice for 15 min

657 and centrifuged at 12,000 x *g* for 10 minutes at 4 °C. The organic (upper) layer was collected,
658 and the aqueous layer was re-extracted with 1 mL of 10:3:2.5 (v/v/v) MTBE/MeOH/water. The
659 MTBE layers were combined for untargeted lipidomic analysis and dried under vacuum. The
660 aqueous layer was centrifuged for 12,000 x *g* for 10 minutes at 4 °C and dried under vacuum.
661 Lipid extracts were reconstituted in 500 µL of 8:2:2 (v/v/v) IPA/ACN/water containing 10 mM
662 ammonium formate and 0.1% formic acid. Concurrently, a process blank sample was prepared
663 and then a pooled quality control (QC) sample was prepared by taking equal volumes (~50 µL)
664 from each sample after final resuspension.

665

666 ***LC-MS Analysis and Data Processing***

667 Lipid extracts were separated on an Acquity UPLC CSH C18 column (2.1 x 100 mm; 1.7 µm)
668 coupled to an Acquity UPLC CSH C18 VanGuard precolumn (5 x 2.1 mm; 1.7 µm) (Waters,
669 Milford, MA) maintained at 65 °C connected to an Agilent HiP 1290 Sampler, Agilent 1290
670 Infinity pump, and Agilent 6545 Accurate Mass Q-TOF dual AJS-ESI mass spectrometer
671 (Agilent Technologies, Santa Clara, CA). Samples were analyzed in a randomized order in both
672 positive and negative ionization modes in separate experiments acquiring with the scan range
673 *m/z* 100 – 1700. Mobile phase A consisted of ACN:H₂O (60:40, v/v) in 10 mM ammonium
674 formate and 0.1% formic acid, and mobile phase B consisted of IPA:ACN:H₂O (90:9:1, v/v/v) in
675 10 mM ammonium formate and 0.1% formic acid. For negative mode analysis the modifiers
676 were changed to 10 mM ammonium acetate. The chromatography gradient for both positive and
677 negative modes started at 15% mobile phase B then increased to 30% B over 2.4 min, it then
678 increased to 48% B from 2.4 – 3.0 min, then increased to 82% B from 3 – 13.2 min, then
679 increased to 99% B from 13.2 – 13.8 min where it's held until 16.7 min and then returned to the
680 initial conditions and equilibrated for 5 min. Flow was 0.4 mL/min throughout, with injection
681 volumes of 2 µL for positive and 10 µL negative mode. Tandem mass spectrometry was
682 conducted using iterative exclusion, the same LC gradient at collision energies of 20 V and 27.5

683 V in positive and negative modes, respectively. For data processing, Agilent MassHunter (MH)
684 Workstation and software packages MH Qualitative and MH Quantitative were used. The
685 pooled QC ($n = 8$) and process blank ($n = 4$) were injected throughout the sample queue to
686 ensure the reliability of acquired lipidomics data. For lipid annotation, accurate mass and
687 MS/MS matching was used with the Agilent Lipid Annotator library and LipidMatch (64). Results
688 from the positive and negative ionization modes from Lipid Annotator were merged based on
689 the class of lipid identified. Data exported from MH Quantitative was evaluated using Excel
690 where initial lipid targets are parsed based on the following criteria. Only lipids with relative
691 standard deviations (RSD) less than 30% in QC samples are used for data analysis.
692 Additionally, only lipids with background AUC counts in process blanks that are less than 30%
693 of QC are used for data analysis. The parsed excel data tables are normalized based on the
694 ratio to class-specific internal standards, then to tissue mass and sum prior to statistical
695 analysis.

696

697 ***Supplemental Methods***

698 Additional methods are found in the Supplemental Materials.

699

700 ***Statistics***

701 All data presented herein are expressed as mean \pm SEM. The level of significance was set at p
702 < 0.05 . Student's t-tests (2-tailed) were used to determine the significance between
703 experimental groups and two-way ANOVA analysis followed by Tukey's HSD post hoc test was
704 used where appropriate. The sample size (n) for each experiment is shown in the figure legends
705 and corresponds to the sample derived from the individual mice or for cell culture experiments
706 on an individual batch of cells. Unless otherwise stated, statistical analyses were performed
707 using GraphPad Prism software.

708

709 ***Study Approval***

710 Experiments on animals were performed in strict accordance with the Guide for the Care and
711 Use of Laboratory Animals of the National Institutes of Health. All animals were handled
712 according to approved University of Utah Animal Use and Care Committee (IACUC) protocols
713 (#20-07007). The protocol as approved by the Committee on the Ethics of Animal Experiments
714 of the University of Utah.

715

716 ***Data Availability***

717 Data are available in the “Supporting data values” XLS file. RNA sequencing datasets were
718 deposited in GEO (accession number GSE260612).

719

720 ***Author contributions***

721 P.S. contributed to the Conceptualization, Data curation, Formal analysis, Validation,
722 Investigation, Visualization, Methodology, Writing – original draft, Writing – review and editing,
723 Funding acquisition; G.C. contributed to the Conceptualization, Investigation, Data curation,
724 Methodology; A.A.C. contributed to the Conceptualization, Data curation, Formal analysis,
725 Methodology; J.A.M contributed to the Data curation, Formal analysis, Resources; Q.P.
726 contributed to Data curation, Formal analysis, Resources; M.J.L. contributed to the Data
727 curation; M.J. contributed to the Data curation; H.E. contributed to the Data curation; P.J.F.
728 contributed to Data curation; P.C.O. contributed to Data curation; Z.S.M. contributed to the
729 Conceptualization, Methodology; A.D.P. contributed to Data curation; S.W. contributed to Data
730 curation; M.A.W. contributed to Data curation; E.B.T. contributed to the Methodology; J.E.C.
731 contributed to the Methodology, Resources, Supervision; M.J.D. contributed to the
732 Conceptualization, Methodology, Resources, Supervision; J.R. contributed to the
733 Conceptualization, Resources; K.F. contributed to the Conceptualization, Formal analysis,

734 Validation, Visualization, Supervision, Writing – review and editing, Resources, Funding
735 acquisition, Project administration.

736

737 **Acknowledgements**

738 This research is supported by National Institutes of Health grants DK107397, DK127979,
739 GM144613, AG074535, AG067186 (to K.F.), DK091317 (to M.J.L.), DK130555 (to A.D.P.),
740 DK104998 (to E.B.T.), AG076075, AG079477, AG050781 (to M.J.D.), GM131854, CA228346
741 (to J.R.), Howard Hughes Medical Institute (J.R.), and American Heart Association grant 915674
742 (to P.S.). University of Utah Metabolomics Core Facility is supported by S10 OD016232, S10
743 OD021505, and U54 DK110858. We would like to thank Nikita Abraham from the University of
744 Utah Molecular Medicine Program for assistance with figures.

745 **References**

- 746 1. Lee IM, Shiroma EJ, Lobelo F, Puska P, Blair SN, Katzmarzyk PT. Effect of physical
747 inactivity on major non-communicable diseases worldwide: an analysis of burden of disease and
748 life expectancy. *The Lancet*. 2012;380(9838):219-29.
- 749 2. Ding D, Lawson KD, Kolbe-Alexander TL, Finkelstein EA, Katzmarzyk PT, van Mechelen
750 W, Pratt M. The economic burden of physical inactivity: a global analysis of major non-
751 communicable diseases. *The Lancet*. 2016;388(10051):1311-24.
- 752 3. Booth FW, Chakravarthy MV, Gordon SE, Spangenburg EE. Waging war on physical
753 inactivity: using modern molecular ammunition against an ancient enemy. *J Appl Physiol* (1985).
754 2002;93(1):3-30.
- 755 4. Booth FW, Laye MJ, Lees SJ, Rector RS, Thyfault JP. Reduced physical activity and risk
756 of chronic disease: the biology behind the consequences. *Eur J Appl Physiol*. 2008;102(4):381-
757 90.
- 758 5. Bowden Davies KA, Sprung VS, Norman JA, Thompson A, Mitchell KL, Halford JCG, et
759 al. Short-term decreased physical activity with increased sedentary behaviour causes metabolic
760 derangements and altered body composition: effects in individuals with and without a first-
761 degree relative with type 2 diabetes. *Diabetologia*. 2018;61(6):1282-94.
- 762 6. Krogh-Madsen R, Thyfault JP, Broholm C, Mortensen OH, Olsen RH, Mounier R, et al. A
763 2-wk reduction of ambulatory activity attenuates peripheral insulin sensitivity. *J Appl Physiol*
764 (1985). 2010;108(5):1034-40.
- 765 7. Dirks ML, Wall BT, van de Valk B, Holloway TM, Holloway GP, Chabowski A, et al. One
766 Week of Bed Rest Leads to Substantial Muscle Atrophy and Induces Whole-Body Insulin
767 Resistance in the Absence of Skeletal Muscle Lipid Accumulation. *Diabetes*. 2016;65(10):2862-
768 75.
- 769 8. Mikines KJ, Richter EA, Dela F, Galbo H. Seven days of bed rest decrease insulin action
770 on glucose uptake in leg and whole body. *J Appl Physiol* (1985). 1991;70(3):1245-54.
- 771 9. Rynders CA, Blanc S, DeJong N, Bessesen DH, Bergouignan A. Sedentary behaviour is
772 a key determinant of metabolic inflexibility. *J Physiol*. 2018;596(8):1319-30.
- 773 10. Bergouignan A, Rudwill F, Simon C, Blanc S. Physical inactivity as the culprit of
774 metabolic inflexibility: evidence from bed-rest studies. *J Appl Physiol* (1985). 2011;111(4):1201-
775 10.
- 776 11. Reidy PT, Monnig JM, Pickering CE, Funai K, Drummond MJ. Preclinical rodent models
777 of physical inactivity-induced muscle insulin resistance: challenges and solutions. *J Appl Physiol*
778 (1985). 2021;130(3):537-44.
- 779 12. Morey-Holton E, Globus RK, Kaplansky A, Durnova G. The hindlimb unloading rat
780 model: literature overview, technique update and comparison with space flight data. *Adv Space*
781 *Biol Med*. 2005;10:7-40.
- 782 13. Marmonti E, Busquets S, Toledo M, Ricci M, Beltra M, Gudino V, et al. A Rat
783 Immobilization Model Based on Cage Volume Reduction: A Physiological Model for Bed Rest?
784 *Front Physiol*. 2017;8:184.
- 785 14. Mahmassani ZS, Reidy PT, McKenzie AI, Petrocelli JJ, Matthews O, de Hart NM, et al.
786 Absence of MyD88 from Skeletal Muscle Protects Female Mice from Inactivity-Induced
787 Adiposity and Insulin Resistance. *Obesity (Silver Spring, Md)*. 2020;28(4):772-82.
- 788 15. Heden TD, Johnson JM, Ferrara PJ, Eshima H, Verkerke ARP, Wentzler EJ, et al.
789 Mitochondrial PE potentiates respiratory enzymes to amplify skeletal muscle aerobic capacity.
790 *Sci Adv*. 2019;5(9):eaax8352.
- 791 16. Shiao YJ, Balcerzak B, Vance JE. A mitochondrial membrane protein is required for
792 translocation of phosphatidylserine from mitochondria-associated membranes to mitochondria.
793 *Biochem J*. 1998;331 (Pt 1)(Pt 1):217-23.

- 794 17. Vance JE. Phospholipid synthesis in a membrane fraction associated with mitochondria.
795 J Biol Chem. 1990;265(13):7248-56.
- 796 18. Kennedy EP, Weiss SB. The function of cytidine coenzymes in the biosynthesis of
797 phospholipides. J Biol Chem. 1956;222(1):193-214.
- 798 19. Vance JE, Steenbergen R. Metabolism and functions of phosphatidylserine. Progress in
799 lipid research. 2005;44(4):207-34.
- 800 20. Zhao T, Goedhart CM, Sam PN, Sabouny R, Lingrell S, Cornish AJ, et al. PISD is a
801 mitochondrial disease gene causing skeletal dysplasia, cataracts, and white matter changes.
802 Life Sci Alliance. 2019;2(2).
- 803 21. Peter VG, Quinodoz M, Pinto-Basto J, Sousa SB, Di Gioia SA, Soares G, et al. The
804 Liberfarb syndrome, a multisystem disorder affecting eye, ear, bone, and brain development, is
805 caused by a founder pathogenic variant in the PISD gene. Genet Med. 2019;21(12):2734-43.
- 806 22. Girisha KM, von Elsner L, Neethukrishna K, Muranjan M, Shukla A, Bhavani GS, et al.
807 The homozygous variant c.797G>A/p.(Cys266Tyr) in PISD is associated with a
808 Spondyloepimetaphyseal dysplasia with large epiphyses and disturbed mitochondrial function.
809 Hum Mutat. 2019;40(3):299-309.
- 810 23. Borkman M, Storlien LH, Pan DA, Jenkins AB, Chisholm DJ, Campbell LV. The relation
811 between insulin sensitivity and the fatty-acid composition of skeletal-muscle phospholipids. N
812 Engl J Med. 1993;328(4):238-44.
- 813 24. Pan DA, Lillioja S, Milner MR, Kriketos AD, Baur LA, Bogardus C, Storlien LH. Skeletal
814 muscle membrane lipid composition is related to adiposity and insulin action. J Clin Invest.
815 1995;96(6):2802-8.
- 816 25. Vessby B, Tengblad S, Lithell H. Insulin sensitivity is related to the fatty acid composition
817 of serum lipids and skeletal muscle phospholipids in 70-year-old men. Diabetologia.
818 1994;37(10):1044-50.
- 819 26. Newsom SA, Brozinick JT, Kiseljak-Vassiliades K, Strauss AN, Bacon SD, Kerege AA,
820 et al. Skeletal muscle phosphatidylcholine and phosphatidylethanolamine are related to insulin
821 sensitivity and respond to acute exercise in humans. J Appl Physiol (1985). 2016;120(11):1355-
822 63.
- 823 27. Alibegovic AC, Hojbjerg L, Sonne MP, van Hall G, Stallknecht B, Dela F, Vaag A.
824 Impact of 9 days of bed rest on hepatic and peripheral insulin action, insulin secretion, and
825 whole-body lipolysis in healthy young male offspring of patients with type 2 diabetes. Diabetes.
826 2009;58(12):2749-56.
- 827 28. Virtue S, Even P, Vidal-Puig A. Below thermoneutrality, changes in activity do not drive
828 changes in total daily energy expenditure between groups of mice. Cell Metab. 2012;16(5):665-
829 71.
- 830 29. Bodine SC, Stitt TN, Gonzalez M, Kline WO, Stover GL, Bauerlein R, et al. Akt/mTOR
831 pathway is a crucial regulator of skeletal muscle hypertrophy and can prevent muscle atrophy in
832 vivo. Nature cell biology. 2001;3(11):1014-9.
- 833 30. Rudwill F, O'Gorman D, Lefai E, Chery I, Zahariev A, Normand S, et al. Metabolic
834 Inflexibility Is an Early Marker of Bed-Rest-Induced Glucose Intolerance Even When Fat Mass Is
835 Stable. J Clin Endocrinol Metab. 2018;103(5):1910-20.
- 836 31. Kelley DE, He J, Menshikova EV, Ritov VB. Dysfunction of mitochondria in human
837 skeletal muscle in type 2 diabetes. Diabetes. 2002;51(10):2944-50.
- 838 32. Holloszy JO. "Deficiency" of mitochondria in muscle does not cause insulin resistance.
839 Diabetes. 2013;62(4):1036-40.
- 840 33. Anderson EJ, Lustig ME, Boyle KE, Woodlief TL, Kane DA, Lin CT, et al. Mitochondrial
841 H₂O₂ emission and cellular redox state link excess fat intake to insulin resistance in both
842 rodents and humans. J Clin Invest. 2009;119(3):573-81.

843 34. Eshima H, Siripoksup P, Mahmassani ZS, Johnson JM, Ferrara PJ, Verkerke ARP, et al.
844 Neutralizing mitochondrial ROS does not rescue muscle atrophy induced by hindlimb unloading
845 in female mice. *J Appl Physiol* (1985). 2020;129(1):124-32.

846 35. Kondo H, Nakagaki I, Sasaki S, Hori S, Itokawa Y. Mechanism of oxidative stress in
847 skeletal muscle atrophied by immobilization. *Am J Physiol*. 1993;265(6 Pt 1):E839-44.

848 36. Dirks ML, Miotto PM, Goossens GH, Senden JM, Petrick HL, van Kranenburg J, et al.
849 Short-term bed rest-induced insulin resistance cannot be explained by increased mitochondrial
850 H₂O₂ emission. *The Journal of Physiology*. 2020;598(1):123-37.

851 37. Ferrara PJ, Rong X, Maschek JA, Verkerke AR, Siripoksup P, Song H, et al.
852 Lysophospholipid acylation modulates plasma membrane lipid organization and insulin
853 sensitivity in skeletal muscle. *J Clin Invest*. 2021;131(8).

854 38. Johnson JM, Ferrara PJ, Verkerke ARP, Coleman CB, Wentzler EJ, Neuffer PD, et al.
855 Targeted overexpression of catalase to mitochondria does not prevent cardioskeletal myopathy
856 in Barth syndrome. *J Mol Cell Cardiol*. 2018;121:94-102.

857 39. Warburg O, Wind F, Negelein E. The Metabolism of Tumors in the Body. *J Gen Physiol*.
858 1927;8(6):519-30.

859 40. Vander Heiden MG, Cantley LC, Thompson CB. Understanding the Warburg effect: the
860 metabolic requirements of cell proliferation. *Science*. 2009;324(5930):1029-33.

861 41. Bricker DK, Taylor EB, Schell JC, Orsak T, Boutron A, Chen YC, et al. A mitochondrial
862 pyruvate carrier required for pyruvate uptake in yeast, *Drosophila*, and humans. *Science*.
863 2012;337(6090):96-100.

864 42. Herzig S, Raemy E, Montessuit S, Veuthey JL, Zamboni N, Westermann B, et al.
865 Identification and functional expression of the mitochondrial pyruvate carrier. *Science*.
866 2012;337(6090):93-6.

867 43. Hildyard JC, Ammala C, Dukes ID, Thomson SA, Halestrap AP. Identification and
868 characterisation of a new class of highly specific and potent inhibitors of the mitochondrial
869 pyruvate carrier. *Biochim Biophys Acta*. 2005;1707(2-3):221-30.

870 44. Divakaruni AS, Rogers GW, Murphy AN. Measuring Mitochondrial Function in
871 Permeabilized Cells Using the Seahorse XF Analyzer or a Clark-Type Oxygen Electrode. *Curr*
872 *Protoc Toxicol*. 2014;60:25 2 1-16.

873 45. Booth FW, Roberts CK, Laye MJ. Lack of exercise is a major cause of chronic diseases.
874 *Compr Physiol*. 2012;2(2):1143-211.

875 46. Selathurai A, Kowalski GM, Burch ML, Sepulveda P, Risis S, Lee-Young RS, et al. The
876 CDP-Ethanolamine Pathway Regulates Skeletal Muscle Diacylglycerol Content and
877 Mitochondrial Biogenesis without Altering Insulin Sensitivity. *Cell Metab*. 2015;21(5):718-30.

878 47. Funai K, Lodhi IJ, Spears LD, Yin L, Song H, Klein S, Semenkovich CF. Skeletal Muscle
879 Phospholipid Metabolism Regulates Insulin Sensitivity and Contractile Function. *Diabetes*.
880 2016;65(2):358-70.

881 48. Arikkeeth D, Nelson R, Vance JE. Defining the importance of phosphatidylserine
882 synthase-1 (PSS1): unexpected viability of PSS1-deficient mice. *J Biol Chem*.
883 2008;283(19):12888-97.

884 49. Bergo MO, Gavino BJ, Steenbergen R, Sturbois B, Parlow AF, Sanan DA, et al. Defining
885 the importance of phosphatidylserine synthase 2 in mice. *J Biol Chem*. 2002;277(49):47701-8.

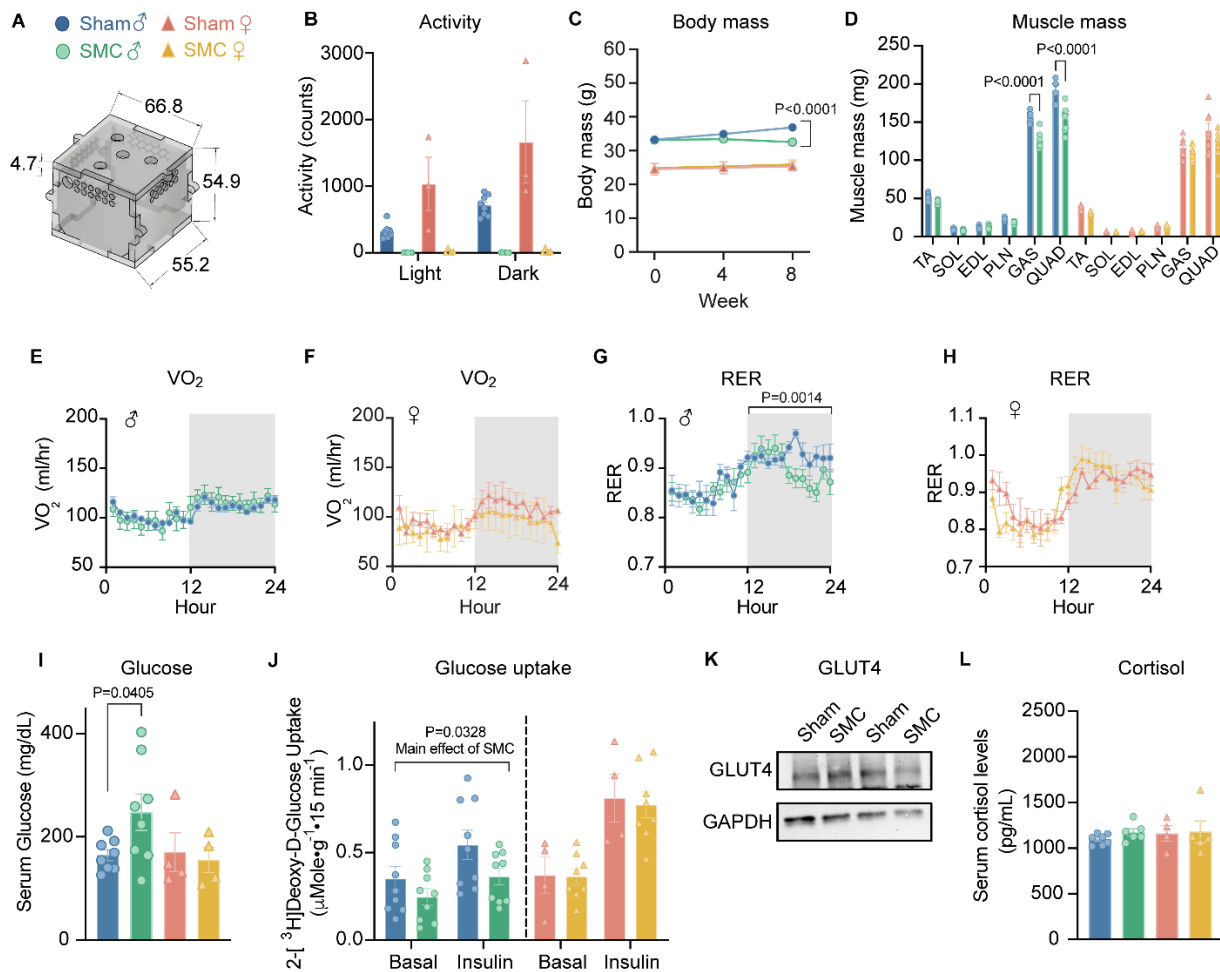
886 50. Miyata N, Watanabe Y, Tamura Y, Endo T, Kuge O. Phosphatidylserine transport by
887 Ups2-Mdm35 in respiration-active mitochondria. *J Cell Biol*. 2016;214(1):77-88.

888 51. Calzada E, Avery E, Sam PN, Modak A, Wang C, McCaffery JM, et al.
889 Phosphatidylethanolamine made in the inner mitochondrial membrane is essential for yeast
890 cytochrome bc1 complex function. *Nat Commun*. 2019;10(1):1432.

891 52. Lee K, Kerner J, Hoppel CL. Mitochondrial carnitine palmitoyltransferase 1a (CPT1a) is
892 part of an outer membrane fatty acid transfer complex. *J Biol Chem*. 2011;286(29):25655-62.

- 893 53. Heden TD, Neuffer PD, Funai K. Looking Beyond Structure: Membrane Phospholipids of
894 Skeletal Muscle Mitochondria. *Trends Endocrinol Metab.* 2016;27(8):553-62.
- 895 54. McGarry JD, Mannaerts GP, Foster DW. A possible role for malonyl-CoA in the
896 regulation of hepatic fatty acid oxidation and ketogenesis. *J Clin Invest.* 1977;60(1):265-70.
- 897 55. McGarry JD, Brown NF. The mitochondrial carnitine palmitoyltransferase system. From
898 concept to molecular analysis. *Eur J Biochem.* 1997;244(1):1-14.
- 899 56. Bensard CL, Wisidagama DR, Olson KA, Berg JA, Krah NM, Schell JC, et al. Regulation
900 of Tumor Initiation by the Mitochondrial Pyruvate Carrier. *Cell Metab.* 2020;31(2):284-300 e7.
- 901 57. Cluntun AA, Badolia R, Lettlova S, Parnell KM, Shankar TS, Diakos NA, et al. The
902 pyruvate-lactate axis modulates cardiac hypertrophy and heart failure. *Cell Metab.*
903 2021;33(3):629-48 e10.
- 904 58. Choi CS, Kim YB, Lee FN, Zabolotny JM, Kahn BB, Youn JH. Lactate induces insulin
905 resistance in skeletal muscle by suppressing glycolysis and impairing insulin signaling. *Am J*
906 *Physiol Endocrinol Metab.* 2002;283(2):E233-40.
- 907 59. Olsen RH, Krogh-Madsen R, Thomsen C, Booth FW, Pedersen BK. Metabolic
908 responses to reduced daily steps in healthy nonexercising men. *JAMA.* 2008;299(11):1261-3.
- 909 60. Coker RH, Hays NP, Williams RH, Wolfe RR, Evans WJ. Bed rest promotes reductions
910 in walking speed, functional parameters, and aerobic fitness in older, healthy adults. *J Gerontol*
911 *A Biol Sci Med Sci.* 2015;70(1):91-6.
- 912 61. Sternfeld B, Dugan S. Physical activity and health during the menopausal transition.
913 *Obstet Gynecol Clin North Am.* 2011;38(3):537-66.
- 914 62. Lark DS, Torres MJ, Lin CT, Ryan TE, Anderson EJ, Neuffer PD. Direct real-time
915 quantification of mitochondrial oxidative phosphorylation efficiency in permeabilized skeletal
916 muscle myofibers. *Am J Physiol Cell Physiol.* 2016;311(2):C239-45.
- 917 63. Matyash V, Liebisch G, Kurzchalia TV, Shevchenko A, Schwudke D. Lipid extraction by
918 methyl-tert-butyl ether for high-throughput lipidomics. *J Lipid Res.* 2008;49(5):1137-46.
- 919 64. Koelmel JP, Kroeger NM, Gill EL, Ulmer CZ, Bowden JA, Patterson RE, et al. Expanding
920 Lipidome Coverage Using LC-MS/MS Data-Dependent Acquisition with Automated Exclusion
921 List Generation. *J Am Soc Mass Spectrom.* 2017;28(5):908-17.

922



923

924 **Figure 1: SMC housing induces metabolic inflexibility in male but not female mice. (A)**

925 Small mouse cage schematic. (B) Activity counts of sham and small mouse cage (SMC) mice

926 via indirect calorimetry (*n* = 8 per group). (C) Body mass time course (*n* = 6-14 per group). (D)

927 Skeletal muscle tissue mass (*n* = 7-8 per group). (E) Absolute VO₂ of male sham and SMC mice

928 via indirect calorimetry (*n* = 8-9 per group). (F) Absolute VO₂ of female sham and SMC mice via

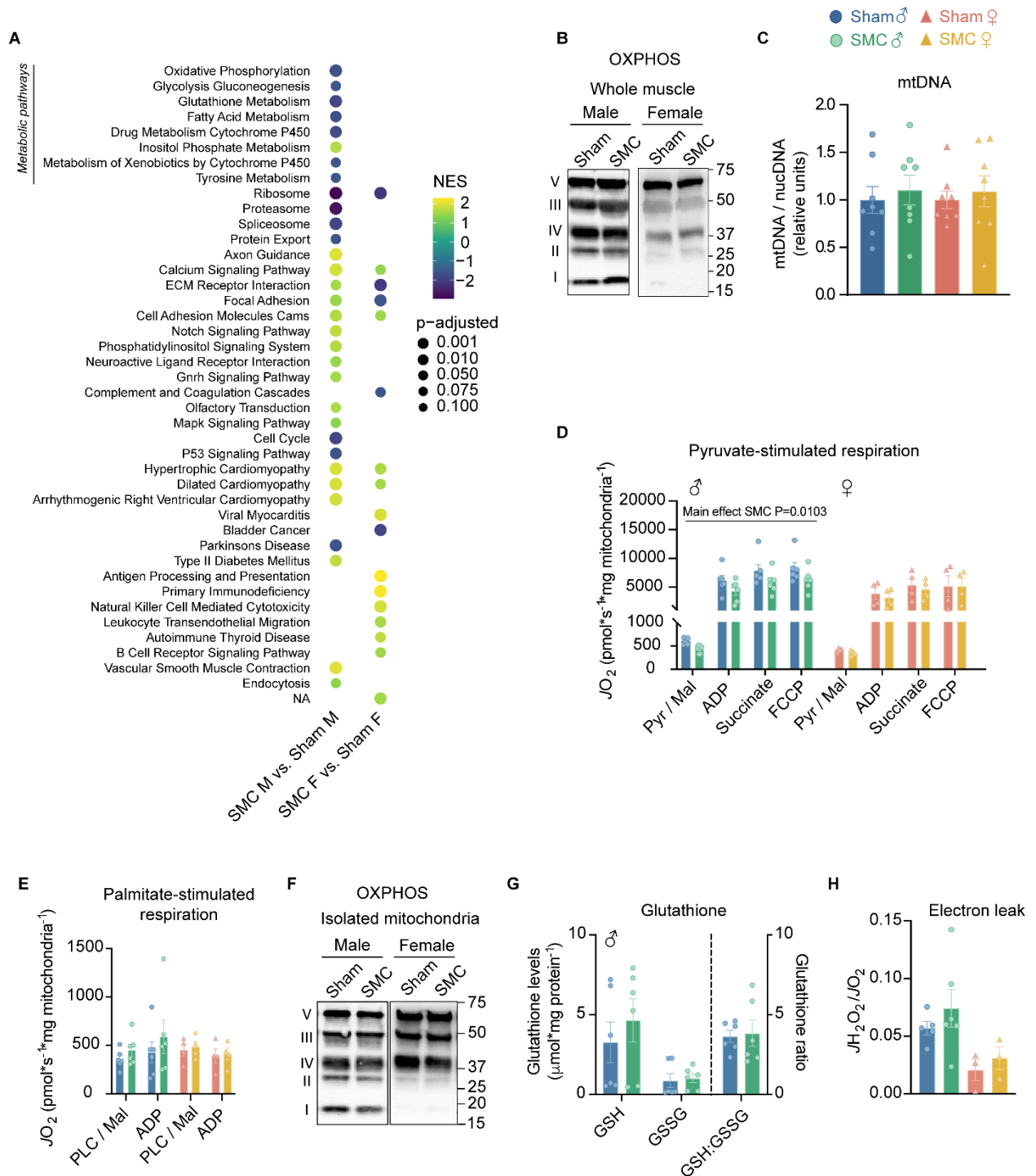
929 indirect calorimetry (*n* = 3-4 per group). (G) Respiratory exchange ratio (RER) of male sham and

930 SMC mice (*n* = 8-9 per group). (H) RER of female sham and SMC mice (*n* = 3-4 per group). (I)

931 Fasting serum glucose levels of sham and SMC mice (*n* = 4-8 per group). (J) [³H]2-

932 deoxyglucose glucose uptake in soleus muscles of male and female sham and SMC mice with

933 or without 200 μ U/mL of insulin ($n = 4-9$ per group). (K) GLUT4 and GAPDH protein abundance
934 in gastrocnemius muscles. (L) Circulating cortisol levels from male and female sham and SMC
935 mice ($n = 4-7$ per group). TA: tibialis anterior; SOL: soleus; EDL: extensor digitorum longus;
936 PLN: plantaris; GAS: gastrocnemius; QUAD: quadriceps; iWAT: inguinal white adipose tissue;
937 gWAT: gonadal white adipose tissue. Data represent mean \pm SEM. P-values generated by two-
938 tailed, equal variance, Student's t-test (D), or by 2-way ANOVA with Tukey's post hoc test (B-C,
939 E-H, and I).
940



941

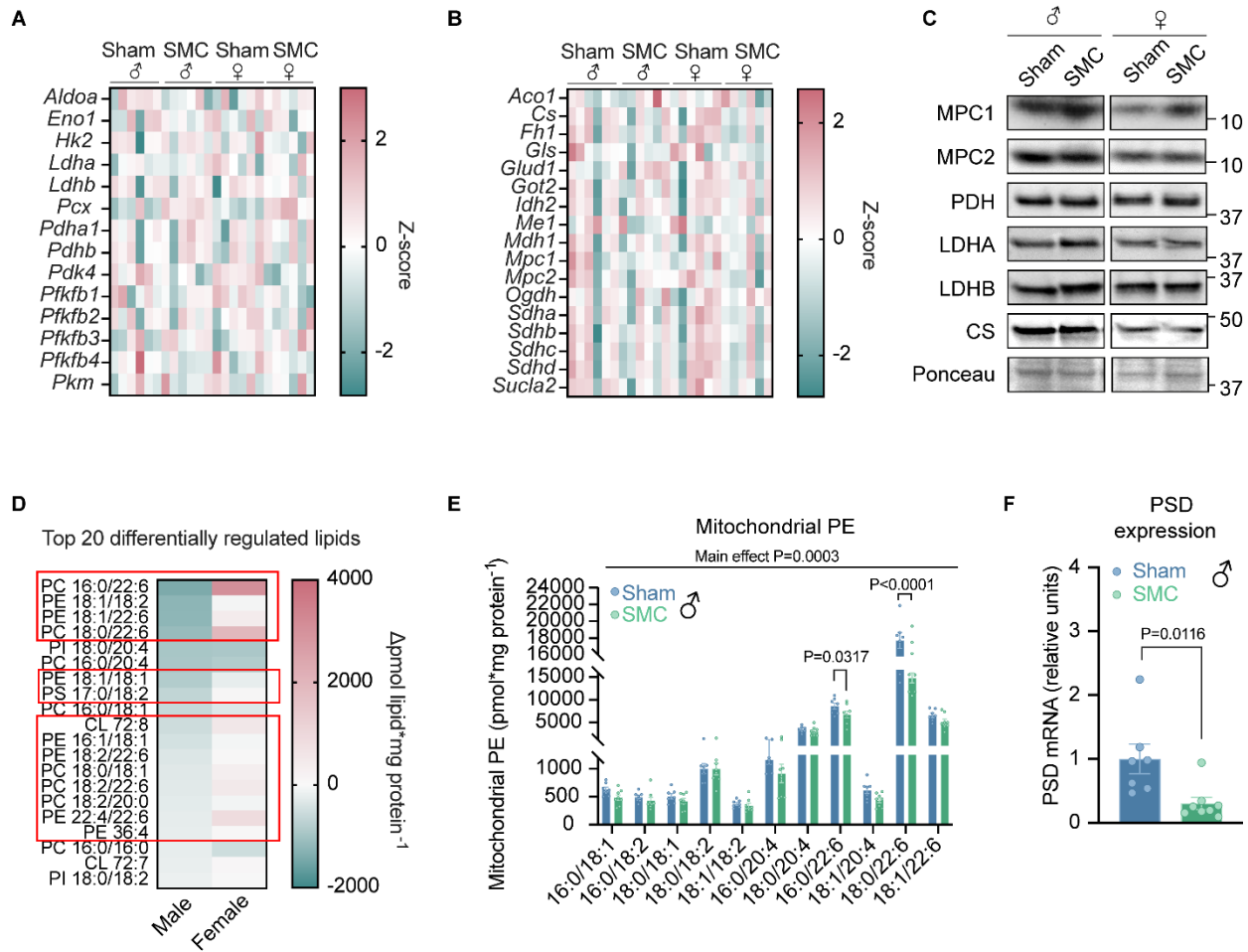
942 **Figure 2: SMC housing reduces pyruvate-dependent respiration without altering**

943 **palmitate-stimulated respiration.** (A) Dot plot representing gene set enrichment analysis

944 (GSEA) pathway analysis (Kyoto Encyclopedia of Genes and Genomes (KEGG)) of differentially

945 expressing genes (FDR < 0.05) in skeletal muscle of sham and small mouse cage (SMC) mice.

946 Normalized enrichment scores are represented by a darker color (negatively enriched) and
947 lighter color (positively enriched), while a larger dot diameter indicates a smaller p-adjusted
948 value. Dot plot was generated with R Studio. (B) Representative western blot of respiratory
949 complexes (I-V) of whole muscle tissue of sham and SMC mice ($n = 3-4$ per group). (C) Ratio of
950 nuclear to mitochondrial DNA in gastrocnemius muscle ($n = 8$ per group). (D) O_2 utilization in
951 isolated mitochondria from gastrocnemius muscle measured in the presence of 2 mM ADP, 0.5
952 mM malate (Mal), 5 mM pyruvate (Pyr), 10 mM succinate, 1 μ M carbonyl cyanide-*p*-
953 trifluoromethoxyphenylhydrazone (FCCP) of sham and SMC mice ($n = 4-6$ per group). (E) O_2
954 utilization in isolated mitochondria measured in the presence of 2 mM ADP (adenosine
955 diphosphate), 0.5 mM malate, 0.02 mM palmitoyl-L-carnitine (PLC) ($n = 4-6$ per group). (F)
956 Representative western blot of respiratory complex proteins in isolated muscle mitochondria of
957 sham and SMC mice ($n = 5-6$ per group). (G) Reduced (GSH) and oxidized (GSSG) glutathione
958 levels in plantaris muscle of sham and SMC mice ($n = 6$ per group). (H) Electron leak ($J_{H_2O_2}/$
959 O_2) with succinate in isolated muscle mitochondria from gastrocnemius muscle of sham and
960 SMC mice ($n = 3-6$ per group). Data represent mean \pm SEM. P-values generated by 2-way
961 ANOVA with Tukey's post hoc test (C-E, G, and H).
962



963

964 **Figure 3: Physical inactivity by SMC housing alters skeletal muscle membrane lipid**

965 **composition.** (A) Heat map of glycolytic genes in sham and small mouse cage (SMC) mice ($n =$

966 6 per group). (B) Heat map of tricarboxylic acid (TCA) cycle genes in sham and SMC mice ($n =$

967 6 per group). (C) Representative western blots of glycolytic/TCA genes in sham and SMC mice

968 ($n = 5-7$ per group). (D) Top 20 differentially regulated skeletal muscle (gastrocnemius)

969 mitochondrial lipids between SMC and sham mice ($n = 7-8$ per group). The red box highlights

970 the lipids whose change in abundances are unique to male mice. (E) Skeletal muscle

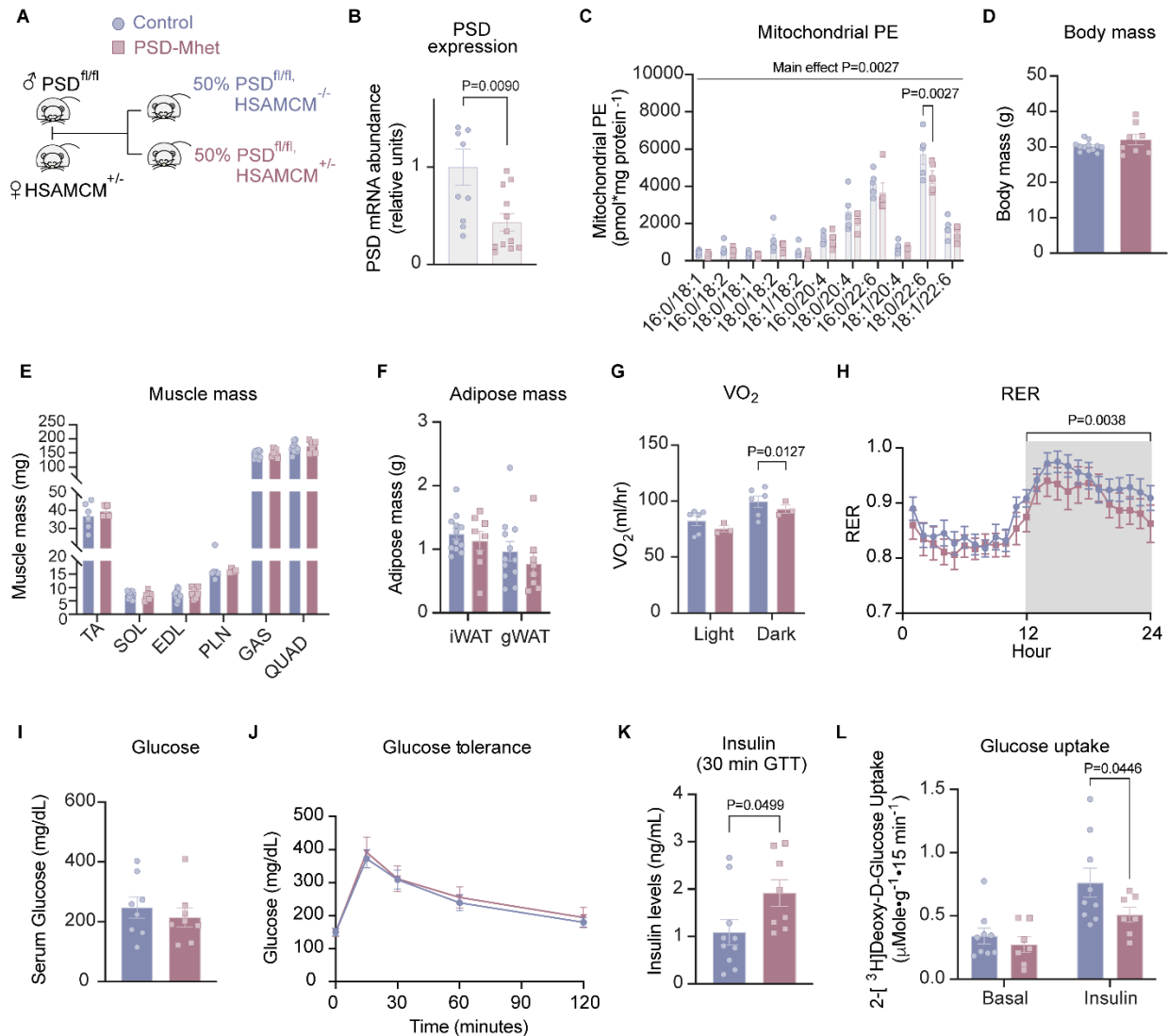
971 mitochondrial PE species (gastrocnemius) of sham and SMC mice ($n = 8$ per group). (F)

972 Skeletal muscle phosphatidylserine decarboxylase (PSD) mRNA levels of sham and SMC mice

973 ($n = 7-8$ per group). MPC1: mitochondrial pyruvate carrier complex 1; MPC2: mitochondrial

974 pyruvate carrier complex 2; PDH: pyruvate dehydrogenase; LDHA: lactate dehydrogenase

975 isoform A; LDHB: lactate dehydrogenase isoform B; CS: citrate synthetase. Data represent
976 mean \pm SEM. P-values generated by two-tailed, equal variance, Student's t-test (F), or by 2-way
977 ANOVA with Tukey's post hoc test (A-B and D-E).



978

979 **Figure 4: Muscle PSD haploinsufficiency increases susceptibility of mice to inactivity-**

980 **induced metabolic inflexibility.** (A) Mouse breeding schematic. (B) phosphatidylserine

981 decarboxylase (PSD) mRNA levels of sham Cre control and PSD-Mhet (PSD muscle-specific

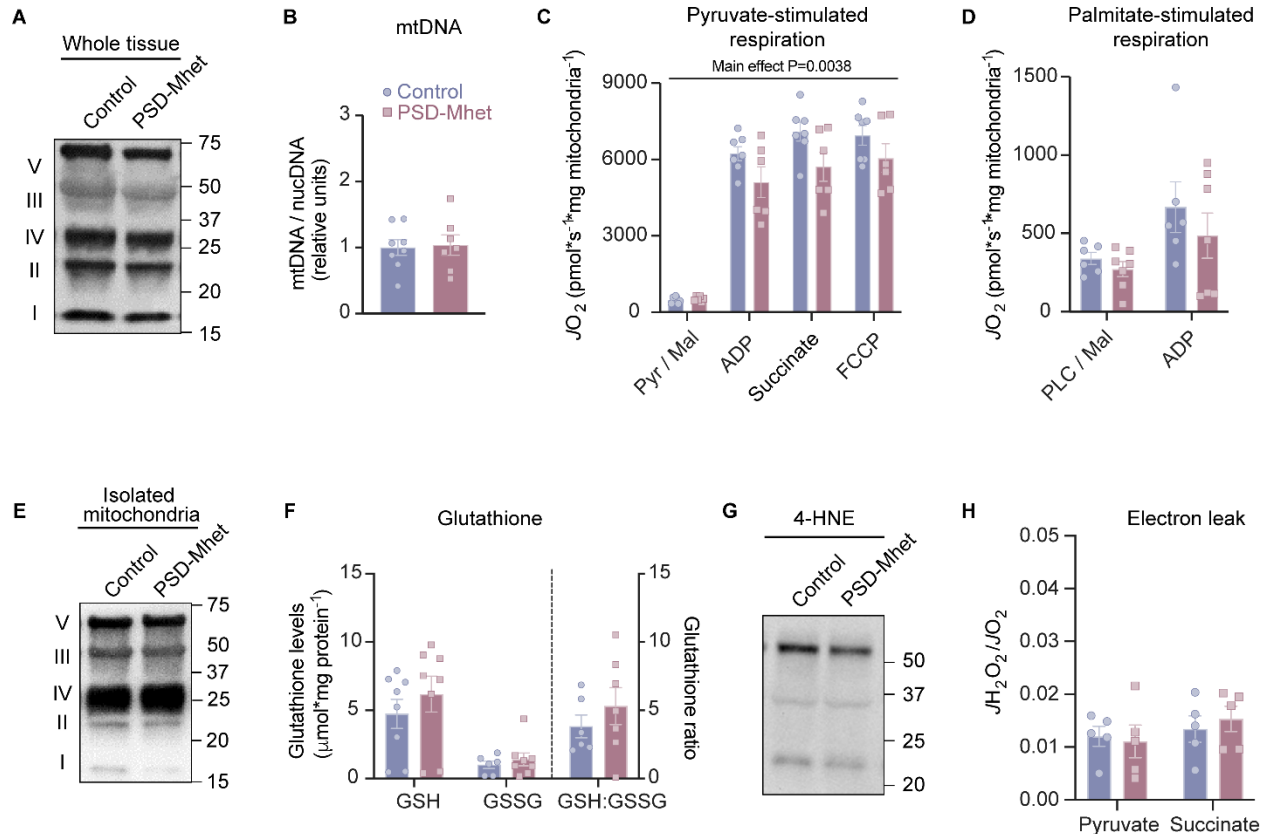
982 heterozygous knockout) mice ($n = 11-12$ per group). (C) Muscle mitochondrial PE levels (from

983 gastrocnemius muscles) of sham control and PSD-Mhet mice ($n = 5$ per group). (D) Body mass

984 of small mouse cage (SMC) Control and SMC PSD-Mhet mice after 8 weeks of reduced activity

985 ($n = 8-12$ per group). Skeletal muscle (E) and adipose masses (F) after SMC intervention ($n = 8-$

986 12 per group). (G) Absolute VO_2 via indirect calorimetry ($n = 3-6$ per group). (H) Respiratory
987 exchange ratio (RER) ($n = 8-11$ per group). (I) Serum glucose levels ($n = 8$ per group). (J)
988 Glucose tolerance test (GTT) performed around Week 7 of SMC intervention ($n = 8-13$ per
989 group). (K) Serum insulin levels taken at the 30-minute time point during the GTT ($n = 8-10$ per
990 group). (L) [3H]2-deoxyglucose glucose uptake in soleus muscles after 8 weeks of SMC ($n = 7-9$
991 per group). TA: tibialis anterior; SOL: soleus; EDL: extensor digitorum longus; PLN: plantaris;
992 GAS: gastrocnemius; QUAD: quadriceps; iWAT: inguinal white adipose tissue; gWAT: gonadal
993 white adipose tissue. All data are from male control and PSD-Mhet mice. Data represent mean
994 \pm SEM. P-values generated by two-tailed, equal variance, Student's t-test (B, D, I, and K), or by
995 2-way ANOVA with Tukey's post hoc test (C, E-H, J, and L).
996



997

998 **Figure 5: Diminished mitochondrial pyruvate respiration by PSD haploinsufficiency is not**

999 **mediated by oxidative stress.** (A) Representative western blot of respiratory protein

1000 complexes (I-V) of whole gastrocnemius muscle of small mouse cage (SMC) Control and SMC

1001 PSD-Mhet (PSD muscle-specific heterozygous knockout) mice ($n = 4-7$ per group). (B) Nuclear

1002 to mitochondrial DNA in gastrocnemius muscles ($n = 8$ per group). (C) O₂ utilization in isolated

1003 muscle mitochondria from gastrocnemius muscles with tricarboxylic acid (TCA) cycle substrates

1004 using the same conditions described earlier ($n = 6-7$ per group). (D) O₂ utilization in isolated

1005 muscle mitochondria from gastrocnemius muscles with fatty acid substrates using the same

1006 conditions described earlier ($n = 6-7$ per group). (E) Representative western blot of respiratory

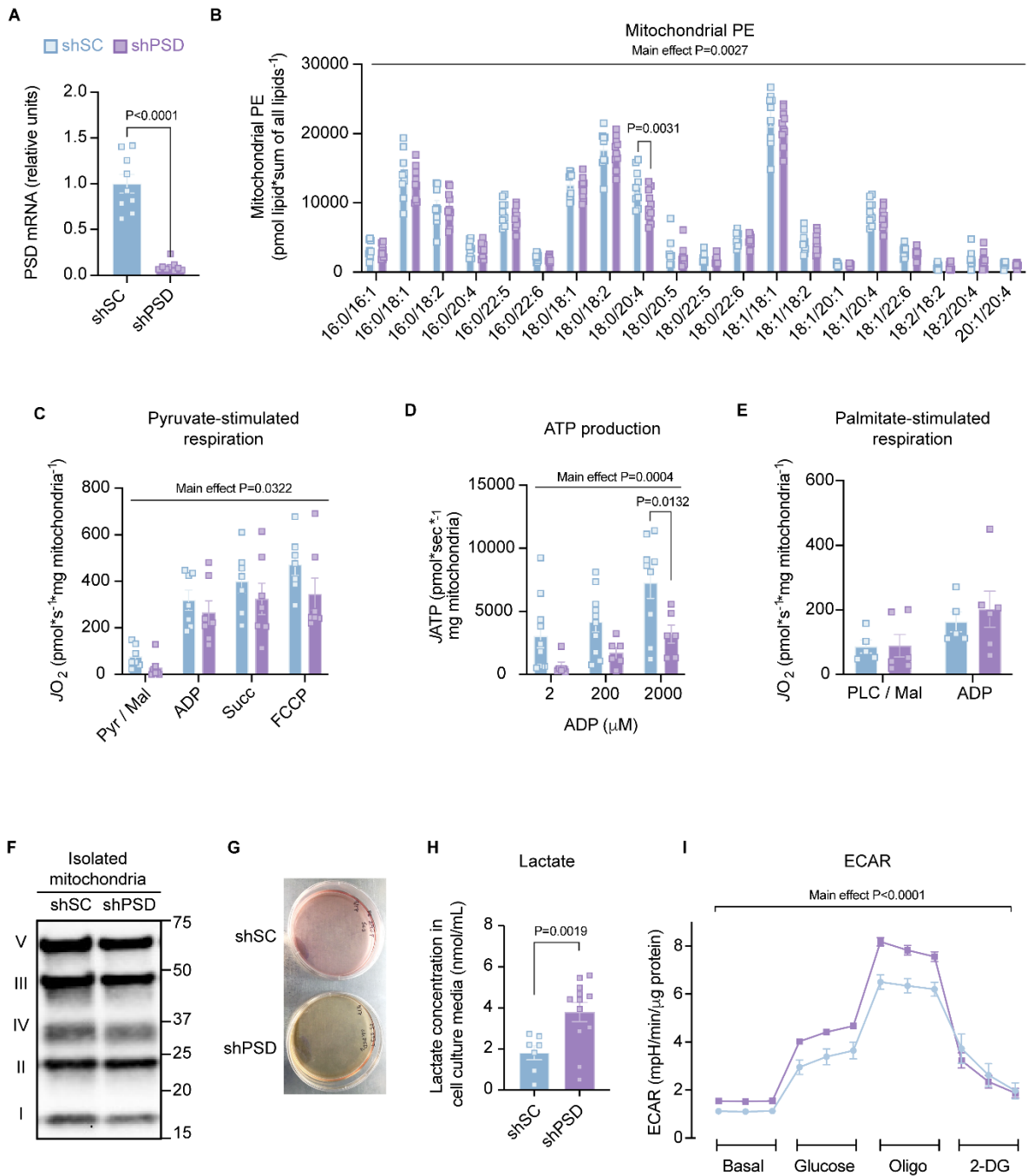
1007 complexes (I-V) of isolated muscle mitochondria from gastrocnemius muscles of SMC Control

1008 and SMC PSD-Mhet mice ($n = 5$ per group). (F) Reduced (GSH) and oxidized (GSSG)

1009 glutathione levels in plantaris levels ($n = 8$ per group). (G) Representative 4-hydroxynonenal (4-

1010 HNE) western blot of whole muscle of SMC Control and SMC PSD-Mhet mice ($n = 6$ per group).

1011 (H) Electron leak in isolated muscle mitochondria from gastrocnemius muscles stimulated with
1012 succinate or pyruvate (Pyr) and auranofin ($n = 5$ per group). PLC: palmitoyl-L-carnitine; ADP:
1013 adenosine diphosphate; FCCP: carbonyl cyanide-*p*-trifluoromethoxyphenylhydrazone. All data
1014 are from male control and PSD-Mhet mice. Data represent mean \pm SEM. P-values generated by
1015 two-tailed, equal variance, Student's t-test (B), or by 2-way ANOVA with Tukey's post hoc test
1016 (C-D, F, and H).
1017



1018

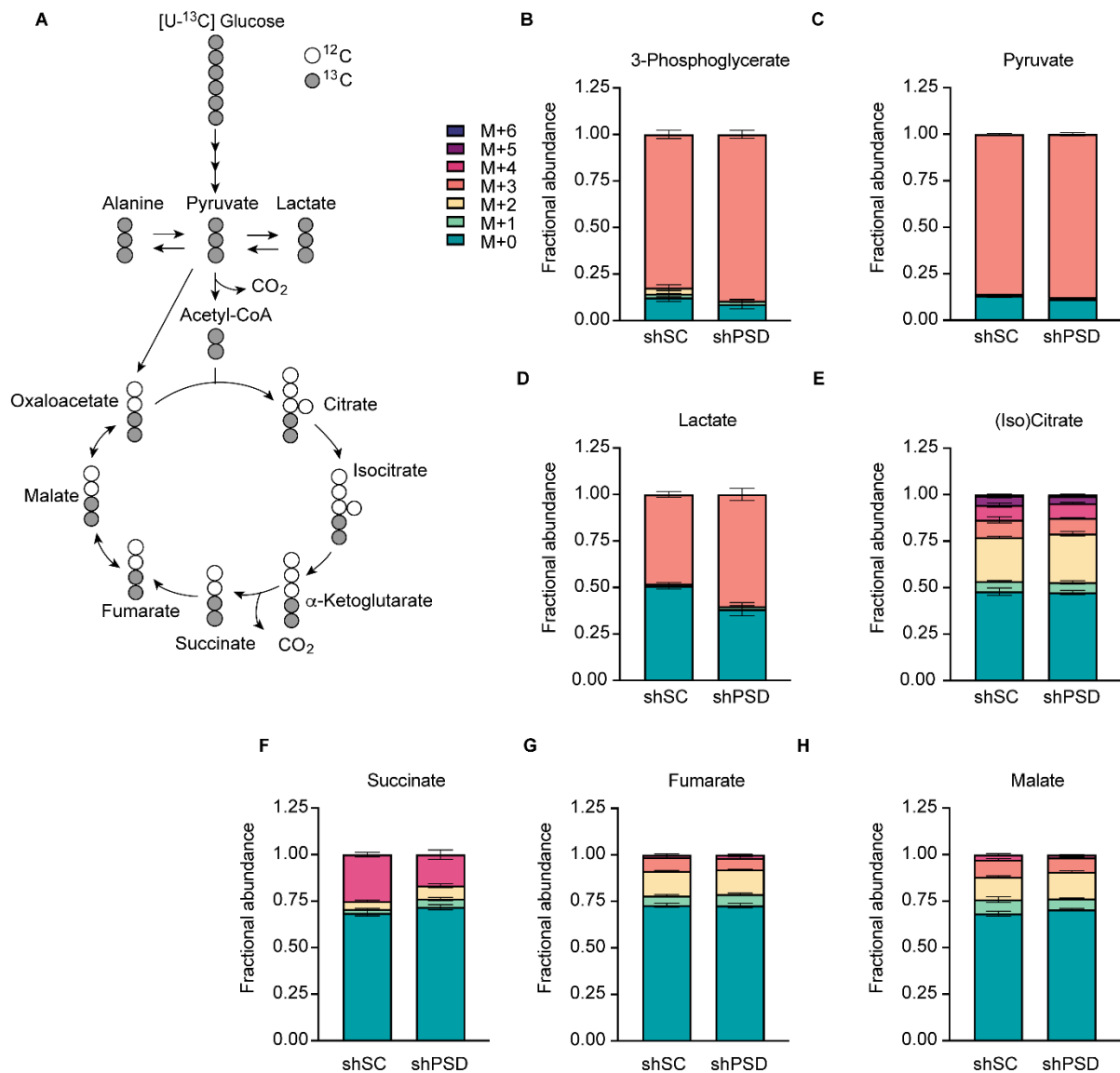
1019 **Figure 6: Mitochondrial PE deficiency impairs pyruvate metabolism. (A)**

1020 Phosphatidylserine decarboxylase (PSD) mRNA abundance in scrambled control (shSC) and

1021 PSD knockdown (shPSD) C2C12 myotubes ($n = 9$ per group). (B) Phosphatidylethanolamine

1022 (PE) levels from isolated mitochondria of shSC and shPSD cells ($n = 9-10$ per group). (C) O_2

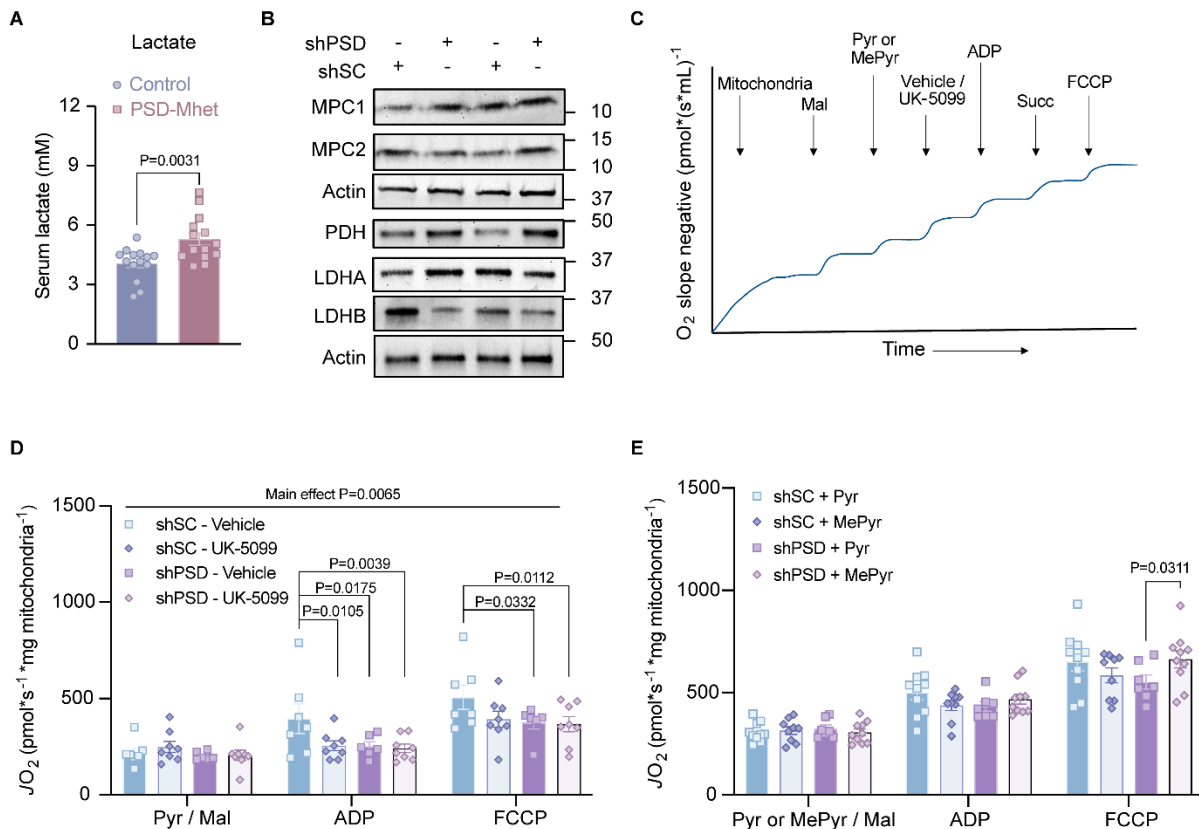
1023 consumption with Krebs cycle substrates using the same conditions described earlier ($n = 7$ per
1024 group). (D) ATP (adenosine triphosphate) production from isolated mitochondria of shSC and
1025 shPSD myotubes measured in the presence of 0.5 mM malate (Mal), 5 mM pyruvate (Pyr), 10
1026 mM succinate (Succ) and either 2, 200, or 2000 μ M ADP (adenosine diphosphate) ($n = 7-10$ per
1027 group). (E) O_2 consumption with fatty acid substrates using the same conditions described
1028 earlier ($n = 5-6$ per group). (F) Representative western blot of respiratory complexes I-V in
1029 isolated mitochondria from shSC and shPSD cells ($n = 5-6$ per group). (G) Representative
1030 image of media color from cell culture plates. (H) Quantification of lactate production in the
1031 media after 24 hours ($n = 7-12$ per group). (I) Seahorse extracellular acidification rate (ECAR) (n
1032 = 10 replicates per group). PLC: palmitoyl-L-carnitine; Oligo: oligomycin; 2DG: 2-deoxyglucose.
1033 Data represent mean \pm SEM. P-values generated by two-tailed, equal variance, Student's t-test
1034 (A and H), or by 2-way ANOVA with Tukey's post hoc test (B-E and I).
1035



1036

1037 **Figure 7: PSD knockdown increases lactate flux.** (A) Atom mapping for $[U-^{13}C_6]$ -glucose
 1038 tracing incorporation into glycolytic and Krebs cycle intermediates. White circles represent ^{12}C
 1039 atoms, while black circles signify ^{13}C atoms. Isotope labeling pattern between scrambled control
 1040 (shSC) and PSD knockdown (shPSD) myotubes for intracellular (B) 3-phosphoglycerate, (C)
 1041 pyruvate, (D) lactate, (E) (iso)citrate, (F) succinate, (G) fumarate, and (H) malate ($n = 4-5$ per
 1042 group). CO_2 : carbon dioxide. Data represent mean \pm SEM.

1043



1044

1045 **Figure 8: Mitochondrial PE facilitates pyruvate entry.** (A) Circulating lactate levels from SMC

1046 control and PSD-Mhet mice (*n* = 14 per group). (B) Representative western blot of MPC1,

1047 MPC2, PDH, LDHA, LDHB, and Actin between scrambled control (shSC) and PSD knockdown

1048 (shPSD) C2C12 myotubes (*n* = 6 per group). (C) A schematic for the order in which UK-5099 or

1049 methyl pyruvate were injected during high-resolution respirometry experiments. (D) Pyruvate-

1050 dependent O₂ consumption in isolated mitochondria from shSC and shPSD myotubes in the

1051 presence or absence of the MPC inhibitor, UK-5099 (100 nm) and the same Krebs cycle

1052 substrate conditions described above (*n* = 6-8 per group). (E) Pyruvate-dependent respiration in

1053 isolated mitochondria with Krebs cycle substrate conditions described above with either

1054 pyruvate or methyl pyruvate as a substrate (*n* = 6-10 per group). MPC1: mitochondrial pyruvate

1055 carrier complex 1; MPC2; mitochondrial pyruvate carrier complex 2; PDH: pyruvate

1056 dehydrogenase; LDHA: lactate dehydrogenase isoform A; LDHB: lactate dehydrogenase

- 1057 isoform B. Data represent mean \pm SEM. P-values generated by Student's t-test (A) or 2-way
1058 ANOVA with Tukey's post hoc test (D-E).